Correlations & Transport Properties of Ultracold Atomic Gases in Optical Lattices

Diploma Thesis

Felix Schmitt

July 2005

Da endlich sah ich das Pendel. Die Kugel, frei schwebend am Ende eines langen metallischen Fadens, der hoch in der Wölbung des Chores befestigt war, beschrieb ihre weiten konstanten Schwingungen mit majestätischer Isochronie.
Ich wusste – doch jeder hätte es spüren müssen im Zauber dieses ruhigen Atems –, daß die Periode geregelt wurde durch das Verhältnis der Quadratwurzel aus der Länge des Fadens zu jener Zahl π, die, irrational für die irdischen Geister, in göttlicher Ratio unweigerlich den Umfang mit dem Durchmesser eines jeden möglichen Kreises verbindet, dergestalt, daß die Zeit dieses Schweifens einer Kugel von einem Pol zum anderen das Ergebnis einer geheimen Verschwörung der zeitlosesten aller Maße war – der Einheit des Aufhängepunktes, der Zweiheit einer abstrakten Dimension, der Dreizahl von π, des geheimen Vierecks der Wurzel und der Perfektion des Kreises. [...] Die Erde rotierte, doch der Ort, wo das Pendel verankert war, war der einzige Fixpunkt im Universum.

Umberto Eco,
Das Foucaultsche Pendel

Summary

Ultracold atomic gases in optical lattices are an unique toolbox to study various phenomena in strongly correlated quantum systems. Furthermore, they are a perfect realisation of the Hubbard model. We utilise this model to describe the zero temperature behaviour of single component bosonic gases, as well as fermion-fermion and boson-fermion mixtures. Using an exact diagonalisation of the respective Hamilton matrices via Lanczos algorithms we are able to compute the groundstate and a few lowest eigenvalues for moderate system sizes. After an introduction and a short historical overview, we provide, in chapter 2, the physical toolbox needed to approach the problem. Chapter 3 discusses bosonic systems to get a first impression of the underlying physics. We introduce several observables, among these are the condensate fraction, the interference pattern and the fringe visibility, which are directly accessible in experiments, but also the superfluid fraction which is an order parameter for the superfluid to Mott-insulator transition. It turns out that superfluidity has to be clearly distinguished from condensation. Inspired by recent experiments in the group of Immanuel Bloch, we investigate the influence of an external trapping potential on the fringe visibilities and present an explanation for the characteristic kinks. In chapter 4 we use the Hubbard model to describe fermion-fermion mixtures. Our main focus is on several correlation functions – and therefore density matrices – in order to provide a detailed insight into two-particle properties in coordinate as well as in momentum space. In the regime of attractive fermion-fermion interactions we observe a correlation of particles in coordinate space. This long-range pair-coherence is accompanied by correlations in momentum space such that particles of different species and opposite momentum form pairs. For repulsive interactions, where half-filled systems undergo an insulator transition, the anticorrelations in momentum space reveal that this behaviour is triggered by a mutual blocking of quasimomentum single-particle states. As an outlook, chapter 5 combines bosonic and fermionic aspects and presents an example of a system with mixed quantum statistics. We explore the rich phase diagram and mark several particular regions that are of quite different nature. With the help of the two-particle correlations we are able to identify a region where particles of different species exhibit a spatial separation and a second region where they tend to occupy the lattice sites alternately. We also point out some major differences to fermion-fermion systems caused by the mixed statistics.

Contents

Chapter 1

Introduction

In 1924 Satyendra Nath Bose published a derivation of Planck's law by using statistical mechanics of an ideal photon gas. His achievement was not to follow the standard way using statistical independent particles, but independent phase-space cells instead. Unfortunately, he was not well known in the community by then and the work did not attain the deserved attention. He approached his friend Albert Einstein, who immediately noticed the potential of that idea and generalised the theory to gases. Within the same year, Albert Einstein predicted a possible condensation of particles into the energetically lowest single-particle state – the Bose-Einstein condensation. In superconductivity, discovered by Heike Kamerlingh Onnes in 1911 in ultracold mercury, Albert Einstein saw a first hint of an experimental realisation of Bose-Einstein condensation. No more than 33 years later, in 1957, Bardeen, Schrieffer and Cooper were able to give a theoretical explanation of superconductivity. It turned out that the condensation of electron-electron (Cooper) pairs is responsible for the superconducting state in ordinary superconductors.

The first experimental realisation of a pure Bose-Einstein condensate was achieved in 1995 by Eric Cornell and Carl Wieman (National Institute of Standards and Technology, NIST [1]) and Wolfgang Ketterle (Massachusetts Institute of Technology, MIT [2]) using dilute gases of neutral atoms. In the experiment at NIST they used a dilute gas of ^{87}Rb atoms. The laser-cooled atoms were confined in a magnetic trap. By using a rf-evaporation cooling technique a temperature of 170 nK was reached and the condensate emerged. Cornell, Wieman and Ketterle received the Nobel Price in 2001. Since that time much manpower has been spent to develop this interesting field of physics.

By now laboratories all over the world are able to produce Bose-Einstein condensates. The current low temperature record, set by the MIT group, is about 500 pK [3]. As the simple creation of a BEC was no longer the ultimate goal, one started to examine the condensate in more detail. For example, one used a laser beam to stir the condensate and observed the onset of superfluid vortices [4].

Recently, the main focus shifted away from the pure condensates towards strongly correlated boson, boson-fermion, and fermion-fermion systems. By using Feshbach resonances one can tune the interaction between atoms over a wide range, even switching from attractive to repulsive interactions. In such systems it is possible to observe a BEC-BCS crossover [5] that is of particular interest in connection with high-temperature superconductivity. An alternative approach to strongly correlated systems is the application of an optical lattice. Those tunable lattice structures produced by counterpropagating laser beams and loaded with an ultracold gas provide an unique quantum mechanical toolbox. This environment is the perfect experimental realisation of the Hubbard model. A groundbreaking experiment was the observation of the superfluid to Mott-insulator quantum phase transition – predicted by Dieter Jaksch et al. in 1998 [6] and experimentally observed by Markus Greiner et al. in 2001 [7]. The superfluid to Mott-insulator transition was also observed in a one-dimensional lattice by Thilo Stöferle et al. [8]. Various tools for probing the systems in the different quantum phases have been developed, ranging form the observation of matter-wave interference patterns [7] to excitation spectra as a response to lattice modulations [9]. Moreover, different lattice geometries are considered, even disordered random lattices are under investigation [11].

All these experimental achievements were accompanied by an active theoretical development. For example, the Gross-Pitaevskii ansatz was successful in describing pure Bose-Einstein condensates and superfluid vortices [10]. In the strongly correlated regimes, i.e., in optical lattices, mean-field calculations are widely used due to their small computational effort and easy handling. There are more sophisticated methods like Monte Carlo, DMRG and exact diagonalisation techniques that all have assets and drawbacks. We will use the exact diagonalisation of the Hamilton matrix to obtain groundstates and their corresponding energies. This method is able to provide exact – within the framework of the model – results across the whole phase diagram, from the superfluid state to the Mott-insulating state. However, the disadvantage is that we are restricted in system size and, therefore, have to consider finite-size effects.

We use the capabilities of the Hubbard model and the exact diagonalisation of the resulting Hamilton matrix to describe ultracold bosons as well as fermion-fermion and boson-fermion mixtures in optical lattices. In chapters 2 and 3 we introduce the relevant physics and present results for bosonic systems. Furthermore, in chapter 4 we apply the Hubbard model to fermion-fermion mixtures in order to examine similar observables, but also to obtain a detailed insight into two-particle correlations in coordinate as well as in momentum space. It turns out that besides the trivial conducting state at zero fermion-fermion interaction, there are two more characteristic states. For attractive interactions a state with nonvanishing conductivity and strong two-particle pairing in momentum space emerges. In the regime of repulsive interactions a mutual blocking of quasimomentum states leads to a vanishing conductivity. As an outlook we present in chapter 5 the application of the Hubbard model to a system with mixed quantum statistics and point out some major differences to the previously discussed cases. Details on the numerical implementation and the computer codes in general can be found in appendix A.

Chapter 2

Periodic Lattices & Hubbard Model

2.1 Lattice & Bloch Theory

Because we are dealing with many-particle systems in periodic lattice potentials, it is useful to give a brief summary of Bloch's Theory. We will introduce a suitable basis for our problem and define a quantity called 'quasimomentum'. For simplicity we restrict ourselves to a description in 1D.

Assume a potential $V_0(x)$ proportional to $\sin^2(\pi/a\ x)$ which we usually call lattice-potential or simply lattice. For every periodic potential one can find a translation a such that any vector from one position in the lattice to another with exactly the same physical properties is given by $R \equiv l \cdot a$ in which $l\ \in \mathbb{N}$. In our 1D potential that simply could be a shift from one lattice site to another, implying that a is the smallest nonzero vector, called lattice vector. The absolute value of the lattice vector is called the lattice constant or the lattice spacing. Now we define a translation operator $T_R\, f(x) \equiv f(x+R)$ that shifts any function $f(x)$ by the vector R. Note that this is not an operator acting on the Hilbert space. In the case of periodic boundary conditions and a lattice of length $L = Ia$, where I is the number of lattice sites, one finds the identity

$$(T_a)^I\, f(x) = f(x+L) = f(x) \quad \text{or} \quad (T_a)^I = 1\ . \tag{2.1}$$

The complex roots are

$$T_a^{(j)} = e^{\mathbf{i}\frac{2\pi}{I}j} \quad \text{with} \quad j = 0, 1, 2, .., I-1\ . \tag{2.2}$$

Thus, we find for a shift R through the lattice

$$\begin{aligned} T_R\, f(x) &= e^{\mathbf{i}k_j R}\, f(x) \\ &= (T_a^{(j)})^l\, f(x) = e^{\mathbf{i}(\frac{2\pi}{I}\, j\; l)}\, f(x) = e^{\mathbf{i}k_j\; a\, l}\, f(x)\;. \end{aligned} \tag{2.3}$$

In general $k_j \equiv \frac{2\pi}{Ia} j$ has the dimension 1/length and R has the dimension length. We see that the function $f(x)$ is characterised by the index k_j. Hence, we use k_j to label the function $f_{k_j}(x)$.

The wavefunction $\psi(x)$ used to describe a particle in the lattice has to obey equation (2.1). In the following form it does:

$$\psi_{k_j}(x) \equiv e^{\mathbf{i}k_j x} \cdot u_{k_j}(x)\;. \tag{2.4}$$

If we require $u_{k_j}(x)$ to follow the periodicy of the lattice this is easy to show:

$$T_R\, \psi_{k_j}(x) = \psi_{k_j}(x+R) = e^{\mathbf{i}k_j(x+R)} \cdot u_{k_j}(x+R) = e^{\mathbf{i}k_j(x+R)} \cdot u_{k_j}(x) = e^{\mathbf{i}k_j R} \psi_{k_j}(x)\;. \tag{2.5}$$

Equation (2.4) is known as *Bloch's theorem*.

To get an impression of the physical meaning of k_j we consider the lattice potential to be constant (e.g. zero), so $u_{k_j}(x) = c$ is also constant and $\psi_{k_j}(x) = e^{\mathbf{i}k_j x} \cdot c$ becomes the wavefunction of a free particle. Thus, k_j is the analogue to the momentum of a free particle for a lattice system and will be called quasimomentum. We will use the common notation $q_j \equiv k_j$ in the following. Notice, however, that (2.4) is not eigenfunction of the free momentum operator.

Considering the periodicity of the Hamilton operator we can easily show that it commutes with the translation operator:

$$T_R\big(H(x)\; \psi_{q_j}(x)\big) = H(x+R)\; \psi_{q_j}(x+R) = H(x)\; \psi_{q_j}(x+R) = H(x)\; T_R\; \psi_{q_j}(x)\;. \tag{2.6}$$

Commuting operators have the same set of eigenfunctions, so we can write down the Schroedinger equation of a single particle in a periodic lattice. In order to have a basis independent notation we will use Dirac's BracKet notation in the following:

$$\hat{H} \mid \psi_{q_j} \rangle = E_{q_j} \mid \psi_{q_j} \rangle\,, \tag{2.7}$$

$$\psi_{q_j}(x) = \langle\, x \mid \psi_{q_j} \,\rangle\,, \tag{2.8}$$

$$H(x)\; \psi_{q_j}(x) = \langle\, x \mid \hat{H} \mid \psi_{q_j} \,\rangle\,. \tag{2.9}$$

Given that the full set of eigenvectors $\mid \psi_{q_j} \rangle$ should form a complete basis, but that there are only a finite number of different quasimomenta q_j, there have to be further sets of orthogonal states with similar q_j. They can be distinguished by an additional index i: $\mid \psi_{q_j}^{(i)} \rangle$ called the energy band index. All of our calculations are performed within the first energy band, so we will drop this index when discussing the results. Nevertheless, it is important to understand the emergence of band structures. The next section will address this question.

2.2 Energy Bands

Numerical solutions of the single-particle problem in a periodic potential show that the energy spectra are not continuous but show gaps in a way that the energies of a complete set of quasimomenta are separated by those gaps. For this reason, one talks about 'energy bands'. The size of gaps that separate different energy bands are of crucial influence on conducting properties of the system.

It is clear that the existence of these energy bands has to emerge somehow in the dispersion relation of the particles. The model of 'quasi-free' particles is an easy way to get a first impression about the dispersion relation of particles in a periodic potential. The idea is to neglect the effect of the potential on the kinetic energy of particles but to take Bragg reflection of the Bloch waves due to the lattice layers into account [12]. The Bragg condition is given by

$$2\,a\,\sin(\beta) = n\,\lambda \tag{2.10}$$

with the lattice spacing a, the angle of incidence β with respect to the normal of the layers and the particle's wavelength λ. In the one-dimensional case $\beta = \pi/2$ and thus the wavevectors $\tilde{q}_n$ that fulfil the Bragg condition are

$$\tilde{q}_n = \frac{2\pi}{\lambda} = \frac{\pi}{a}\,n\ . \tag{2.11}$$

Comparing this to the allowed quasimomenta we see that the Bragg condition is fulfilled for $j = I/2$:

$$q_j = \frac{2\pi}{aI}\,j = \frac{\pi}{a} = \tilde{q}_1 \quad \text{for} \quad j = \frac{I}{2}\ . \tag{2.12}$$

The quasimomenta q_j within the interval $(-\frac{\pi}{a}, \frac{\pi}{a}]$ define the first Brillouin zone. This interval is simply the shifted one we already obtained from the complex roots (2.2).

In conclusion, those Bloch functions that satisfy the Bragg condition are assumed to

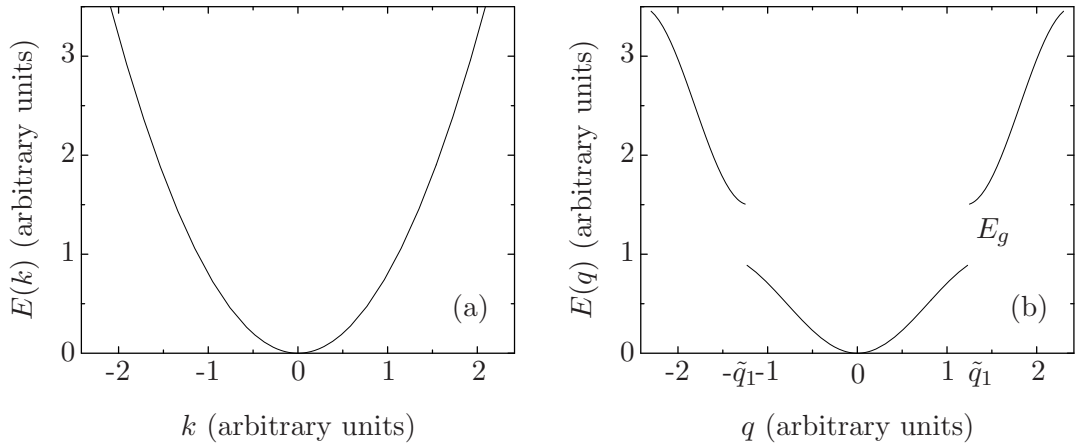

Figure 2.1: (a) Dispersion relation of a free particle $E(k) = k^2/2m$. (b) Dispersion relation of a particle in a periodic potential. Within the simple model discussed in the text, the energy gap E_g at $\tilde{q}_1$ is given by the amplitude A of the lattice potential and appears every time the wavevectors satisfy the Bragg condition.

be no longer propagating but standing waves. The resulting standing-wave wavefunction might be composed of a superposition of a right and a left-travelling Bloch wave $\psi_{\tilde{q}_1}(x)$ with $\tilde{q}_1 = \pm\frac{\pi}{a}$. There are two possibilities to compose this standing wave:

$$\psi^+(x) \;\propto\; e^{\mathbf{i}\,\frac{\pi}{a}\,x} + e^{-\mathbf{i}\,\frac{\pi}{a}\,x} = 2\cos\left(\frac{\pi}{a}\,x\right) \tag{2.13}$$

$$\psi^-(x) \;\propto\; e^{\mathbf{i}\,\frac{\pi}{a}\,x} - e^{-\mathbf{i}\,\frac{\pi}{a}\,x} = 2\mathbf{i}\sin\left(\frac{\pi}{a}\,x\right) . \tag{2.14}$$

If the lattice potential is of the form $V_0(x) = A\,\sin^2(\frac{\pi}{a}x)$, it immediately follows that $\psi^-(x)$ is much higher in energy than $\psi^+(x)$. The energy difference E_g is

$$E_g = \int_0^a V_0(x)\Big(|\psi^-(x)|^2 - |\psi^+(x)|^2\Big)dx = A\;, \tag{2.15}$$

in which we used a normalisation per lattice spacing a for each wavefunction (2.13) and (2.14). Evidently, the dispersion relation of our particles in a periodic potential is similar to the free particle case, except in the vicinity of those wavevectors $\tilde{q}_n$ that are reflected because they satisfy the Bragg condition (figure 2.1).

2.3 Wannier Functions

We saw that Bloch functions form – within a particular energy band – a complete set of functions which build up a basis that describes single particles in a periodic potential.

However, for a description of a many-particle system with contact interactions it is convenient to have a localised basis.

Formally we use an unitary transformation to obtain a basis with spatial quantum numbers ξ_l instead of quasimomentum quantum numbers q_j:

$$w(x-\xi_l) \equiv \frac{1}{\sqrt{I}} \sum_{j=0}^{I-1} e^{-\mathbf{i}q_j\xi_l} \psi_{q_j}(x) \; . \tag{2.16}$$

This transformation leads from the plane-wave-like Bloch functions to functions that are localised at a particular lattice site l. If we consider the lattice wells to be deep, the lattice potential around a given lattice site can be approximated by a harmonic oscillator potential centred at ξ_l: $V_0(\xi_l \pm x) \propto \sin^2(\frac{\pi}{a}(al \pm x)) \approx (\pi^2/a^2)x^2$, where a is the lattice spacing. Therefore, the Wannier functions are to a good approximation harmonic oscillator ground state wavefunctions

$$w(x-\xi_l) \approx (\sigma^2\pi)^{-1/4} \, e^{\frac{-(x-\xi_l)^2}{2\sigma^2}} \; . \tag{2.17}$$

The width parameter σ can be obtained by minimising the energy functional for a given amplitude of the lattice potential. It will turn out that for a description of the Hubbard model there is no need for an explicit form of the Wannier functions because we are able to express the physical properties with the ratio of interaction energy and tunnelling energy alone.

However, for a direct comparison with 'experimental' lattices, we would require the depth and geometry of the lattice potential and the scattering length of the contact interaction in order to calculate the values for the interaction and the tunnelling energy. How this can be done will be shown in section 2.6. Obviously a time dependend description with a varying lattice potential $V_0(x,t)$ leads to a time dependent width of the Gaussion $\sigma(t)$ and thus to time dependent interactions and tunnelling energies. For more details, we refer to [31] and [32].

2.4 Many-Particle Hilbert Space & Number Representation

Because we want to describe more than one particle in a periodic potential we need a quantum mechanical many-particle formulation. The Hilbert space of a N-particle

system $\mathcal{H}^N$ is given by the direct product of the respective single-particle Hilbert spaces $\mathcal{H}_1$ [16]

$$\mathcal{H}^N \equiv \mathcal{H}_1 \otimes \mathcal{H}_1 \otimes \ldots \otimes \mathcal{H}_1 \; . \tag{2.18}$$

The elements of that N-particle Hilbert space are called product states. They are a direct product of N single-particle states, with collective indices ν_i that contain all quantum numbers characterising the state of particle i.

$$\left| \, \nu_1 \, \nu_2 \, \ldots \, \nu_N \, \right\rangle \equiv \left| \, \nu_1 \, \right\rangle \otimes \left| \, \nu_2 \, \right\rangle \otimes \ldots \otimes \left| \, \nu_N \, \right\rangle . \tag{2.19}$$

This particular N-particle Hilbert space, and its elements, know nothing about symmetry or indistinguishability. To allow for this we define an operator $\hat{\mathcal{S}}$ that projects on the symmetric subspace $\mathcal{H}_{\mathcal{S}}^N$ of the N-particle Hilbert space for the description of bosonic particles, and an operator $\hat{\mathcal{A}}$ that projects on the antisymmetric subspace $\mathcal{H}_{\mathcal{A}}^N$ for the description of fermionic particles. For the corresponding symmetrisized and antisymmetrisized many-body states we use the following notation:

$$\left| \, \nu_1 \, \nu_2 \, \ldots \, \nu_N \, \right\rangle_s \;\; \propto \;\; \hat{\mathcal{S}} \left| \, \nu_1 \, \nu_2 \, \ldots \, \nu_N \, \right\rangle , \tag{2.20}$$

$$\left| \, \nu_1 \, \nu_2 \, \ldots \, \nu_N \, \right\rangle_a \;\; \propto \;\; \hat{\mathcal{A}} \left| \, \nu_1 \, \nu_2 \, \ldots \, \nu_N \, \right\rangle . \tag{2.21}$$

In order to explain how these operators work, we will present an example and in addition introduce the number representation of many-body states.

The number representation simply uses the occupation numbers $\{n_1, n_2, \ldots, n_I\}$ of the individual lattice sites to characterise the single-particle Wannier functions appearing in a symmetric (or antisymmetric) many-particle product state. Those states are commonly called Fock states for short. To give an example of a Fock state, consider three bosonic particles $\sum_{l=1}^{I} n_l = N = 3$ on a lattice with four lattice sites $I = 4$. Two particles shall occupy the first site and the third particle the fourth site. The Wannier functions localised at site l are $\left| \, w_l \, \right\rangle$. The many-body wavefunction in coordinate space $\psi(x_1 \, x_2 \, x_3)$ is a symmetrised product of the single-particle wavefunctions

$$\begin{aligned}
\psi(x_1 \, x_2 \, x_3) \;\; &= \;\; \left\langle \, x_1 \, x_2 \, x_3 \mid \{2,0,0,1\} \, \right\rangle \\
&\propto \;\; \left\langle \, x_1 \, x_2 \, x_3 \, \right| \hat{\mathcal{S}} \left| \, w_1 \, w_1 \, w_4 \, \right\rangle \\
&\propto \;\; w(x_1 - \xi_1) \, w(x_2 - \xi_1) \, w(x_3 - \xi_4) \\
&\quad + w(x_1 - \xi_1) \, w(x_3 - \xi_1) \, w(x_2 - \xi_4) + w(x_3 - \xi_1) \, w(x_2 - \xi_1) \, w(x_1 - \xi_4) \;\; .
\end{aligned}$$

The antisymmetrisation operator $\hat{\mathcal{A}}$ we have to use to describe fermionic many-body states generates a minus sign each time two particles are exchanged. Hence, the above

Fock state would be zero because of the double occupancy of lattice site 1. We can modify the states by applying creation and annihilation operators

$$\hat{a}_l^\dagger \mid \{n_1, n_2, ..., n_l, ..., n_I\} \rangle \equiv \sqrt{n_l + 1} \mid \{n_1, n_2, ..., n_l + 1, ..., n_I\} \rangle \quad (2.22)$$

$$\hat{a}_l \mid \{n_1, n_2, ..., n_l, ..., n_I\} \rangle \equiv \sqrt{n_l} \mid \{n_1, n_2, ..., n_l - 1, ..., n_I\} \rangle . \quad (2.23)$$

Their commutation relations are:

$$[\hat{a}_l, \hat{a}_m^\dagger] = \delta_{lm} \quad \text{for bosons} \qquad \text{and} \qquad [\hat{a}_l, \hat{a}_m^\dagger]_+ = \delta_{lm} \quad \text{for fermions} . \quad (2.24)$$

The n_l describe the occupation numbers of the l-th lattice site and their sum must be the total number of particles $\sum n_l = N$. The occupation number operator of the l-th lattice site $\hat{n}_l$ is defined as:

$$\hat{n}_l \equiv \hat{a}_l^\dagger \, \hat{a}_l . \quad (2.25)$$

A Fock state is one possible distribution of particles over the different lattice sites. By successive application of creation operators $\hat{a}_l^\dagger$ we can construct any Fock state out of the vacuum state

$$\mid \{n_1, n_2, \ ... \ , n_I\} \rangle \equiv \prod_{l=1}^{I} \frac{1}{\sqrt{n_l!}} \, (\hat{a}_l^\dagger)^{n_l} \mid \varnothing \rangle . \quad (2.26)$$

The sequence of the indices $l = 1, 2, \ ... \ , I$ has to be in a predefined – usually ascending – order because the symmetry properties are now hidden in the commutation relations. In order to point out the influence of anticommutation relations, let us consider a single Fock state of a fermionic system $\mid \{0, 1, 1, 1, ...\} \rangle$ and a pair of operators, usually appearing in the calculation of density matrices, acting on it

$$\begin{aligned} \hat{a}_1^\dagger \, \hat{a}_3 \quad \mid \{0, 1, 1, 1, ...\} \rangle &= \hat{a}_1^\dagger \, \hat{a}_3 \quad \hat{a}_2^\dagger \, \hat{a}_3^\dagger \, \hat{a}_4^\dagger ... \mid \varnothing \rangle \\ &= -\hat{a}_1^\dagger \, \hat{a}_3 \quad \hat{a}_3^\dagger \, \hat{a}_2^\dagger \, \hat{a}_4^\dagger ... \mid \varnothing \rangle \\ &= -\hat{a}_1^\dagger \, (1 - \hat{a}_3^\dagger \hat{a}_3) \, \hat{a}_2^\dagger \, \hat{a}_4^\dagger ... \mid \varnothing \rangle \\ &= -\hat{a}_1^\dagger \ \hat{a}_2^\dagger \, \hat{a}_4^\dagger ... \mid \varnothing \rangle . \end{aligned}$$

The minus sign would not appear if we did not claim an ordered composition of the Fock states (2.26). We have to keep this in mind otherwise strange things will happen. They will be mentioned during the discussion of fermion-fermion systems in section 4.1.

2.5 Operators in Second Quantisation

We can use the creation and annihilation operators to reformulate any operator, e.g., those that contribute to the Hamiltonian, in the language of Second Quantisation [16]. A single-particle operator acting on a N-particle Hilbert space can be written as

$$\begin{aligned} \hat{T} &\equiv \sum_{i=1}^{N} \hat{t}_i \,, \\ \hat{t}_i &\equiv \hat{1} \otimes \hat{1} \otimes .. \underbrace{\hat{t}}_{i} .. \otimes \hat{1} \,. \end{aligned} \tag{2.27}$$

For example, $\hat{t}_i$ could be the one-particle kinetic energy operator and thus $\hat{T}$ would be the kinetic energy of the entire system. Using the completeness relation, one finds:

$$\begin{aligned} \hat{T} &= \hat{1}\,\hat{T}\,\hat{1} \\ &= \sum_{\nu_1..\nu_N} \sum_{\nu'_1..\nu'_N} \mid \nu_1..\nu_N \,\rangle \,\langle\, \nu_1..\nu_N \mid \hat{T} \mid \nu'_1..\nu'_N \,\rangle \,\langle\, \nu'_1..\nu'_N \mid \end{aligned} \tag{2.28}$$

Exemplarily we discuss a fermionic system and therefore project onto the antisymmetric N-particle Hilbert space

$$\hat{\mathcal{A}}\hat{T}\hat{\mathcal{A}} = N/N! \sum_{\nu_2..\nu_N} \sum_{\nu\nu'} \mid \nu, \nu_2..\nu_N \,\rangle_a \,\langle\, \nu \mid \hat{t} \mid \nu' \,\rangle \,{}_a\langle\, \nu', \nu_2..\nu_N \mid \tag{2.29}$$

$$= \sum_{\nu_2<..<\nu_N} \sum_{\nu\nu'} \mid \nu, \nu_2..\nu_N \,\rangle_a \,\langle\, \nu \mid \hat{t} \mid \nu' \,\rangle \,{}_a\langle\, \nu', \nu_2..\nu_N \mid . \tag{2.30}$$

Using the creation (2.22) and annihilation operators (2.23) with respect to the single particle basis $\mid \nu \,\rangle$ one can cast (2.28) into the form that is known as Second Quantisation:

$$\hat{T} = \sum_{\nu\nu'} \,\langle\, \nu \mid \hat{t} \mid \nu' \,\rangle\, \hat{a}^\dagger_\nu \hat{a}_{\nu'} \,. \tag{2.31}$$

Again the symmetry properties are hidden in the commutation relations (2.24).

For a two-body operator the procedure is essentially the same. $\hat{V}_{ij}$ describes the interaction between particles i and j

$$\hat{V} = \frac{1}{2} \sum_{i,j=1}^{N} \hat{V}_{ij} \,.$$

And in Second Quantisation

$$\hat{V} = \sum_{\nu_1<\nu_2} \sum_{\nu'_1<\nu'_2} {}_a\langle\, \nu_1\nu_2 \mid \hat{v} \mid \nu'_1\nu'_2 \,\rangle_a \, \hat{a}^\dagger_{\nu_1} \hat{a}^\dagger_{\nu_2} \hat{a}_{\nu'_2} \hat{a}_{\nu'_1} \,. \tag{2.32}$$

2.6 The Hubbard Model

In 1998, Peter Zoller proposed to apply the Hubbard model to ultracold gases in optical lattices[1] [17]. Despite its simple structure this model is capable to reproduce most of the features of ultracold gases in optical lattices, e.g., the superfluid to Mott-insulator phase transition. Before introducing the Hubbard model, we have to make several remarks: All of our calculations are done for $T = 0$ K and only the lowest energy band is occupied. Therefore, the interaction energy V (2.41) has to be small enough not to populate higher states.

The Hamiltonian of a sinusoidal lattice potential $V_0(x)$, a possible external magnetic trapping potential $V_T(x)$ and a two-particle interaction $V(x - x')$ in Second Quantisation reads:

$$\hat{H} = \int dx\ \hat{\Psi}^\dagger(x) \Big(-\frac{\hbar^2}{2m}\nabla^2 + V_0(x) + V_T(x)\Big)\hat{\Psi}(x) \tag{2.33}$$

$$+ \int dx\, dx'\ \hat{\Psi}^\dagger(x)\, \hat{\Psi}^\dagger(x')\, V(x - x')\, \hat{\Psi}(x')\hat{\Psi}(x)\ . \tag{2.34}$$

The field operators can be expressed in terms of the creation and annihilation operators with respect to the Wannier functions

$$\hat{\Psi}^\dagger(x) = \sum_{l=1}^{I} \hat{a}_l^\dagger w^*(x - \xi_l)\ , \tag{2.35}$$

$$\hat{\Psi}(x) = \sum_{l=1}^{I} \hat{a}_l w(x - \xi_l)\ . \tag{2.36}$$

The Wannier functions can be chosen to be real, and the two-particle interaction can be written as a contact interaction $V(x - x') = \frac{4\pi a_s}{2m}\delta(x - x')$ with scattering length a_s. Thus, the Hamiltonian with respect to the occupation number representation reads:

$$\hat{H} = \sum_{l,m=1}^{I} \int dx\ \hat{a}_l^\dagger w(x - \xi_l) \left(-\frac{\hbar^2}{2m}\nabla^2 + V_0(x) + V_T(x) \right) \hat{a}_m w(x - \xi_m) \tag{2.37}$$

$$+\frac{4\pi a_s}{2m} \sum_{l,m,n,o=1}^{I} \int dx\ \hat{a}_l^\dagger w(x - \xi_l)\, \hat{a}_m^\dagger w(x - \xi_m)\, \hat{a}_n w(x - \xi_n)\, \hat{a}_o w(x - \xi_o)\ . \tag{2.38}$$

The Hubbard Hamiltonian is composed of three major parts. We will see this if we split the first integral of the Hamiltonian (2.37) – that we call $\tilde{J}_{lm}$ for the moment – into two

[1] He received the Max-Planck-Medal for his work in 2005

parts. One that includes terms of the sum with $l \neq m$ and is called $J_{\{lm\}}$, the other that terms those parts with $l = m$ is referred to as $\epsilon_{l=m}$

$$\tilde{J}_{lm} \equiv J_{\{lm\}} + \epsilon_{l=m} \ .$$

One can see that $J_{\{lm\}}$ describes the tunnelling of particles between different lattice sites. The tunnelling energy $J_{\{lm\}}$ is sometimes called the Josephson[2] energy

$$J_{\{lm\}} \equiv \int dx \ w(x-\xi_l) \left(-\frac{\hbar^2}{2m}\nabla^2 + V_0(x) + V_T(x) \right) w(x-\xi_m) \quad \text{for} \quad l \neq m \ . \tag{2.39}$$

Although the trapping potential term $V_T(x)$ is included, its contribution to the tunnelling energy can be neglected for small distance tunnelling processes because its variation is negligible on the scale of the lattice spacing. The physical meaning of $J_{\{lm\}}$ is not obvious. If we consider $J_{\{lm\}}$ to be the dominant term in (2.42), particles are free to tunnel through the lattice, thus they are highly delocalised and the system has small kinetic energy. In the case of V_l (2.41) being the dominant term, tunnelling is suppressed and particles are strongly localised causing large kinetic energy contributions. This is the reason why $J_{\{lm\}}$ enters with a minus sign to the Hubbard Hamiltonian. Using the argument that the overlap of wavefunctions at adjacent sites is small and therefore the overlap to non-adjacent sites is negligible, we will take into account nearest neighbour hopping only ($|l-m| = 1$). Considering our lattice to be translatorial invariant, $J_{\{lm\}}$ will no longer have indices.

The $\epsilon_{l=m}$ term describes an external trapping potential, e.g., a magnetic dipole trap needed to confine the system. The kinetic energy and the lattice potential are equal at each lattice site and constitute a constant energy offset ΔE for $l = m$. We can set Δ E to zero without restrictions[3]

$$\begin{aligned} \epsilon_l \equiv \epsilon_{l=m} \quad &= \quad \int dx \ V_T(x) |w(x-\xi_l)|^2 \\ &\quad + \underbrace{\int dx \ w(x-\xi_l) \left(-\frac{\hbar^2}{2m}\nabla^2 + V_0(x) \right) w(x-\xi_l)}_{=\Delta E} \ . \end{aligned} \tag{2.40}$$

Note that the ϵ_l term keeps hold of its indices because it depends on the position.

[2] Josephson junctions describe two superconducting areas, separated by a normal conducting area that can be overcome by tunnelling. One might consider the Hubbard model as a line-up of such elements.

[3] We used this ΔE to solve the eigensystem in Mathematica because Mathematica's eigenproblem solver cannot compute the smallest algebraic eigenvalues but the smallest absolute eigenvalues. The Lanczos algorithm used for all calculations shown here does not suffer from this restriction.

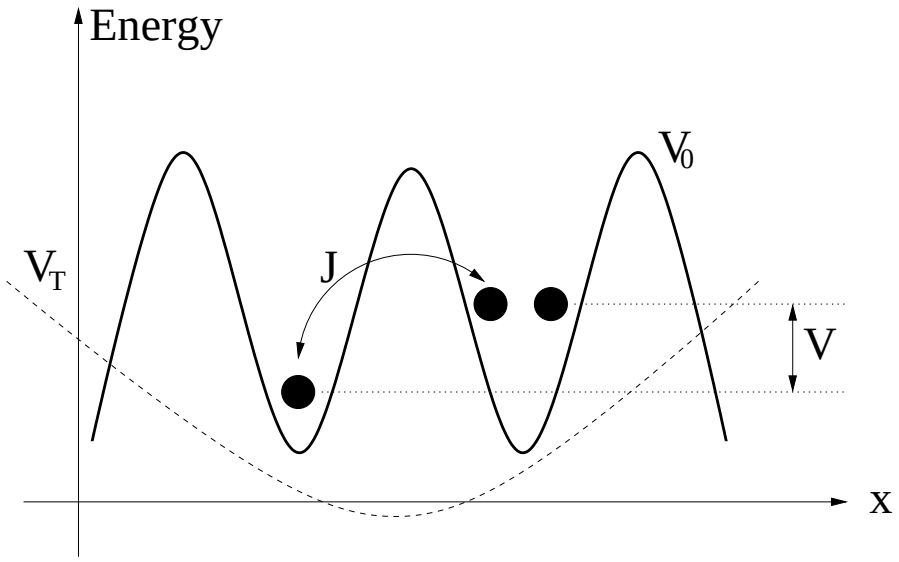

Figure 2.2: Illustration of the parameters of the Hubbard Model. V_0 is the lattice potential, J is the tunnelling energy, V the two-particle interaction energy, and V_T a possible external trapping potential.

The third contribution comes from is the last part of the Hamiltonian (2.38), a two particle interaction energy V_{lmno}. Due to the weak penetration of wavefunctions into adjacent lattice sites we assume in good approximation an on-site contact interaction that is proportional to the probability of finding two particles at the same lattice site l [6]. a_s is the scattering length of the contact interaction

$$V_l \equiv \frac{4\pi a_s}{2m} \int dx \, |w(x - \xi_l)|^4 \, . \tag{2.41}$$

In case of a translationally invariant lattice V_l is also independent of the site index.

The whole situation is sketched in figure 2.2. The dashed line should denote the external trapping potential but is disproportionate. In reality it would show no significant gradient on the scale of two lattice sites.

To recapitulate, the keystone of the Hubbard Hamiltonian is that all relevant physical properties like lattice geometry and scattering length can be parametrised by the ratio of interaction and tunnelling energy V/J and the trapping potential term ϵ_l. We will illustrate this by two examples. First let us assume a shallow lattice potential. The tunnelling energy is large because particles are affected little by the potential. The interaction energy is small because the Wannier functions broaden and thus the integral

over the 4th power of $|w(x-\xi_l)|$ becomes small. That means V/J is small. A deep lattice potential causes a suppression of tunnelling but also Wannier functions of a small width. So the integral over $|w(x-x_l)|^4$ and thus V is larger than in the former case. Therefore V/J is large.

Plugging all these terms together leads to the Hubbard Hamiltonian in second quantisised form:

$$\hat{H} = -J\sum_{l=1}^{I}(\hat{a}_{l+1}^{\dagger}\hat{a}_l + h.a.) + \sum_{l=1}^{I}\epsilon_l\hat{n}_l + \frac{1}{2}V\sum_{l=1}^{I}\hat{n}_l(\hat{n}_l-1)\ . \tag{2.42}$$

By an exact diagonalisation of the Hamilton matrix we obtain a few lowest normalised eigenvectors $\vec{C}^{(\nu)}$ and eigenvalues E_ν

$$\mid \psi_\nu \rangle \;=\; \sum_{\alpha=1}^{D} C_\alpha^{(\nu)} \mid \{n_1,...,n_I\}_\alpha \rangle\ , \tag{2.43}$$

$$\hat{H} \mid \psi_\nu \rangle \;=\; E_\nu \mid \psi_\nu \rangle\ . \tag{2.44}$$

The Hamilton matrix is composed of the on-site energy matrix elements on the diagonal and the hopping elements off the diagonal. D is the dimension of the matrix, i.e., the number of all possible Fock states. The eigenproblem to be solved is of the form:

$$\sum_{\alpha=1}^{D} \langle\ \{n_1,...,n_I\}_\beta \mid \hat{H} \mid \{n_1,...,n_I\}_\alpha\ \rangle\, C_\alpha^{(\nu)} = E_\nu\, C_\beta^{(\nu)}\ . \tag{2.45}$$

Unfortunately, the dimension severely restricts the lattice sizes and particle numbers that can be handled. Some combinatorics leads to the formulas to calculate the basis dimension

$$D \;=\; \frac{(N+I-1)!}{N!(I-1)!} \quad \text{for bosons}\ , \tag{2.46}$$

$$D \;=\; \frac{I!}{N!(I-N)!} \quad \text{for fermions}\ . \tag{2.47}$$

A system of 12 bosons on 12 lattice sites has $D = 1352078$ possible Fock states. Fortunately, the Hamilton matrix is very sparse so we can employ powerful Lanczos algorithms to solve the eigenproblem. Our limitation is not so much CPU power but memory. A single eingenvector of the 12-12-b system stored in double precision uses about 10MB of memory. The Lanczos algorithm allocates about 15 times this memory. Already the dimension of a 14-14-b system is about $D \approx 2\cdot 10^7$. So we would need more than 2GB memory for the diagonalisation.

2.7 Density Matrices

Due to the fact that we will need density matrices in different contexts, we dedicate a separate section to them. We start with the formal definition and then motivate why they are important for our studies.

Let $\left| \psi_\nu \right\rangle$ be an eigenstate of our system as defined in (2.44). In the following discussion we will use a short form for the number basis $\left| \phi_\alpha \right\rangle \equiv \left| \{n_1, ..., n_I\}_\alpha \right\rangle$. The density operator $\hat{\rho}$ of a pure (ground)state is [15]

$$\hat{\rho} \equiv \left| \psi_0 \right\rangle \left\langle \psi_0 \right| . \tag{2.48}$$

The elements of the onebody-density matrix – which is sometimes called first reduced density matrix – $\rho^{(1)}_{ll'}$ are defined as:

$$\begin{aligned} \rho^{(1)}_{ll'} &\equiv \mathrm{Tr}\left(\hat{\rho}\, \hat{a}^\dagger_{l'}\, \hat{a}_l\right) \\ &= \sum_{\alpha=1}^{D} \left\langle \phi_\alpha \mid \psi_0 \right\rangle \left\langle \psi_0 \mid \hat{a}^\dagger_{l'}\, \hat{a}_l \mid \phi_\alpha \right\rangle \\ &= \sum_{\alpha=1}^{D} \left\langle \psi_0 \mid \hat{a}^\dagger_{l'}\, \hat{a}_l \mid \phi_\alpha \right\rangle \left\langle \phi_\alpha \mid \psi_0 \right\rangle \\ &= \left\langle \psi_0 \mid \hat{a}^\dagger_{l'}\, \hat{a}_l \mid \psi_0 \right\rangle . \end{aligned} \tag{2.49}$$

This means we annihilate a particle at lattice site l, create it at site l' and look for the overlap with the original state. The diagonal elements $l = l'$ are simply the occupation numbers. The one-body density matrices are not capable of representing more than single-particle information.

In case we want to probe two-particle features we have to resort to two-body density matrices. If we are dealing with two different particle species, the matrix consists of four blocks. Two blocks connect each species with itself and two symmetric ones mutually connect species with the other. We introduce the latter only. This two-body density matrix in number representation has operators $\hat{a}_l, \hat{a}^\dagger_l$ acting on species 1 and operators $\hat{b}_l, \hat{b}^\dagger_l$ acting on species 2. The corresponding state will be introduced in the discussion of fermion-fermion systems (4.2). So we define the elements of the two-body density matrix:

$$\begin{aligned} \rho^{(2)}_{ll',mm'} &\equiv \mathrm{Tr}\left(\hat{\rho}\, \hat{a}^\dagger_l\, \hat{b}^\dagger_{l'}\, \hat{b}_m\, \hat{a}_{m'}\right) \\ &= \left\langle \psi_0 \mid \hat{a}^\dagger_l\, \hat{b}^\dagger_{l'}\, \hat{b}_m\, \hat{a}_{m'} \mid \psi_0 \right\rangle . \end{aligned} \tag{2.50}$$

To allow for studies of features in momentum space, we will need the quasimomentum density matrices. Thus we have to transform the creation and annihilation operators similar to the unitary transformation from Bloch functions to Wannier functions (2.16).

From Bloch's theorem we know that the dimensionless quasimomenta in our periodic potential with cyclic boundary conditions are of the form $q_j = \frac{2\pi}{I}\, j$. So we obtain the transformed operators [22]:

$$\hat{c}^\dagger_{q_j} \equiv \frac{1}{\sqrt{I}} \sum_{l=1}^{I} e^{-\mathbf{i} q_j l} \hat{a}^\dagger_l \tag{2.51}$$

$$\hat{c}_{q_j} \equiv \frac{1}{\sqrt{I}} \sum_{l=1}^{I} e^{\mathbf{i} q_j l} \hat{a}_l \ . \tag{2.52}$$

For simplicity we will drop the index of q_j in the following and denote $q_2 = \frac{2\pi}{I}\, 2$ by $q = 2$, for example. The quasimomentum one-body density matrix then has the form

$$\begin{aligned}
\tilde{\rho}^{(1)}_{qq'} &= \langle\, \psi_0 \,|\, \hat{c}^\dagger_{q'}\, \hat{c}_q \,|\, \psi_0 \,\rangle && (2.53)\\
&= \frac{1}{I} \langle\, \psi_0 \,|\, \Big(\sum_{l'=1}^{I} e^{-\mathbf{i}\, q'\, l'} \hat{a}^\dagger_{l'} \Big) \Big(\sum_{l=1}^{I} e^{\mathbf{i}\, q\, l} \hat{a}_l \Big) \,|\, \psi_0 \,\rangle && (2.54)\\
&= \frac{1}{I} \langle\, \psi_0 \,|\, \sum_{l',l=1}^{I} \Big(e^{-\mathbf{i}\, q'\, l'} \hat{a}^\dagger_{l'} \cdot e^{\mathbf{i}\, q\, l} \hat{a}_l \Big) \,|\, \psi_0 \,\rangle && (2.55)\\
&= \frac{1}{I} \langle\, \psi_0 \,|\, \sum_{l',l=1}^{I} \Big(e^{\mathbf{i}\,(ql - q'l')} \hat{a}^\dagger_{l'} \hat{a}_l \Big) \,|\, \psi_0 \,\rangle && (2.56)\\
&= \frac{1}{I} \sum_{l',l=1}^{I} e^{\mathbf{i}\,(ql - q'l')} \rho^{(1)}_{ll'} \ . && (2.57)
\end{aligned}$$

This means that we annihilate a particle with quasimomentum q and create one with q'. Keeping in mind that our Hamiltonian is invariant under translation and thus the total (quasi)momentum is conserved, we immediately see that the quasimomentum one-body density matrix cannot have nonvanishing off-diagonal elements. The diagonal elements are again the occupation numbers n_q but in quasimomentum space now

$$\tilde{\rho}^{(1)}_{qq'} = \delta_{qq'}\, n_q \ . \tag{2.58}$$

In the same manner we define the two-body quasimomentum density matrix:

$$\begin{aligned}
\tilde{\rho}^{(2)}_{qq',QQ'} &= \frac{1}{I^2} \left\langle \psi_0 \right| \Big(\sum_{l=1}^{I} e^{-\mathbf{i}\, q\, l} \hat{a}_l^\dagger \Big) \Big(\sum_{l'=1}^{I} e^{-\mathbf{i}\, q'\, l'} \hat{b}_{l'}^\dagger \Big) \Big(\sum_{m'=1}^{I} e^{\mathbf{i}\, Q'\, m'} \hat{a}_{m'} \Big) \Big(\sum_{m=1}^{I} e^{\mathbf{i}\, Q m} \hat{b}_m \Big) \left| \psi_0 \right\rangle \\
&= \frac{1}{I^2} \left\langle \psi_0 \right| \sum_{l,l',m,m'=1}^{I} e^{\frac{2\pi\mathbf{i}}{I}(Q'm'+Qm-ql-q'l')}\, \hat{a}_l^\dagger \hat{b}_{l'}^\dagger \hat{a}_{m'} \hat{b}_m \left| \psi_0 \right\rangle \\
&= \frac{1}{I^2} \sum_{l,l',m,m'=1}^{I} e^{\frac{2\pi\mathbf{i}}{I}\,(Q'm'+Qm-ql-q'l')}\, \rho^{(2)}_{ll',mm'} \,. \qquad (2.59)
\end{aligned}$$

Now let us focus on the physics of these objects. The diagonal elements are easy to understand. In the number representation, those of the one-body density matrix are the mean occupation numbers of the corresponding lattice sites. In an periodic potential without an external trapping potential they all must equal to the filling factor N/I. For the two-body density matrix this is different. If the interaction strength between the particles is attractive they will tend to occupy the same lattice site and thus the inter-species diagonal matrix elements will be larger than in case of repulsive interaction for which particles avoid the company of others.

The off-diagonal elements do not have such an illustrative characteristic. In a perfect condenstate for example all entries of the one-body density matrix in number representation equal 1. This reflects an intrinsic feature of Bose-Einstein condensation because particles that participate in condensation lose their individuality so the wavefunction cannot contain spatial information about those particles.

This characteristic of non-vanishing off-diagonal elements is called 'Off-Diagonal Long-Range Order' (ODLRO). The concept of ODLRO was introduced in a paper by Yang [25]. He proposes that the onset of ODLRO in the n-body density matrices $\rho^{(n)}$ such as the one-body $\rho^{(1)}$ and two-body density matrices $\rho^{(2)}$ leads to a new thermodynamic phase of the system. The conventional Bose-Einstein condensation is a form of ODLRO in $\rho^{(1)}$. There is another but equivalent criterion for ODLRO, the existence of a macroscopic eigenvalue λ_n of the n-body density matrix $\rho^{(n)}$. We will try to motivate this equality. We use the inverse unitary transformation to obtain $\rho^{(1)}$ in number representation. During the discussion of the quasimomentum one-body density matrix we saw

that it only has off-diagonal elements equal zero (2.58). So the sum reduces to

$$\rho^{(1)}_{ll'} = \frac{1}{I} \sum_q n_q \, e^{\mathbf{i}\, q\, (l'-l)} \; . \tag{2.60}$$

The distribution of the quasimomentum occupation numbers is in general given by either Bose or Fermi statistics. Because we work at $T = 0\,K$ we use our knowledge that at large interaction strengths particles are highly located in coordinate space and therefore broad distributed in momentum space. Thus all n_q contribute with small values. In the thermodynamic limit this leads to

$$\rho^{(1)}_{ll'} \longrightarrow 0 \quad \text{as} \quad |l'-l| \longrightarrow \infty \; . \tag{2.61}$$

In our finite systems we have to soften this criterion a little. As we are restricted in size it is impossible perform the thermodynamic limit and thus the off-diagonal elements always remain finite but are orders of magnitude smaller than values near the diagonal in the regime of repulsive interactions.

If we consider a fraction of particles occupying the lowest single particle state, e.g., $n_{q=0} = \alpha N$ we find

$$\rho^{(1)}_{ll'} \longrightarrow \frac{\alpha N}{I} \quad \text{as} \quad |l'-l| \longrightarrow \infty \; . \tag{2.62}$$

The macroscopically occupation of the lowest single-particle energy state is the definition of a Bose-Einstein Condensate [14]. Now let us start conversely and show that the existence of a macroscopic eigenvalue leads to ODLRO.

From Jordan's law we know that every symmetric matrix can be decomposed in a sum over terms consisting of eigenvalues, normalised eigenvectors and their hermitian adjoins. We use this to decompose $\rho^{(1)}_{ll'}$ and sort the terms with respect to the magnitude of the eigenvalues. $\lambda_1 = \alpha N$ shall be the largest eigenvalue and Φ_l the corresponding eigenvector. $\varrho_{ll'}$ shall contain the residual terms

$$\rho^{(1)}_{ll'} = \alpha N \Phi_{l'} \Phi^*_l + \varrho_{ll'} \; . \tag{2.63}$$

Considering the eigenfunctions Φ_l – called 'natural orbitals' – have to reflect the periodicy of the lattice, what is also shown in figure 4.1, and are therefore normalised with a factor proportional $1/\sqrt{I}$ we directly obtain equation (2.62).

The smallest n for which ODLRO appears in the n-body density matrix $\rho^{(n)}$ characterises a 'basic group' of n particles that exhibit ODLRO. For example, in BCS theory

of superconductivity the basic group is made up of two electrons [25]. The largest eigenvalue of the n-body density matrix is usually denoted λ_n. In chapter 3 we will use the largest eigenvalue λ_1 of the one-body density matrix $\rho^{(1)}$ as the criterion for Bose-Einstein condensation.

Chapter 3

Single-Component Bose Gases

As a simple introduction to the applications of the Hubbard model, we will start with some basic observables and – step by step – learn more about the physics of ultracold atomic gases in optical lattices. All following calculations were performed for a commensurate system with $I = 10$ lattice sites and $N = 10$ bosons that has a basis dimension of $D = 92378$ and will be called a '10-10-b' system, and an incommensurate 10-9-b system with a basis dimension $D = 48620$. We employ periodic boundary conditions and no external trapping potential.

3.1 Simple Observables

Once we have obtained the groundstate (2.44), we can compute various observables directly. The simplest one is the mean occupation number [19]

$$n \equiv n_l = \langle \psi \mid \hat{n}_l \mid \psi \rangle . \tag{3.1}$$

It is obvious that the mean occupation number is constant $n_l = N/I$ for lattice sites due to the translatorial symmetry of the lattice. This would be different if we use boxed boundary conditions or an external trapping potential.

Depending on the interaction strength, there are different possible compositions of the eigenstate (2.44) that lead to the same mean occupation number. A quantity that is able to observe differences in these compositions is the fluctuation σ of the mean occupation number [19]

$$\sigma^2 \equiv \langle \psi \mid \hat{n}^2 \mid \psi \rangle - \langle \psi \mid \hat{n} \mid \psi \rangle^2 . \tag{3.2}$$

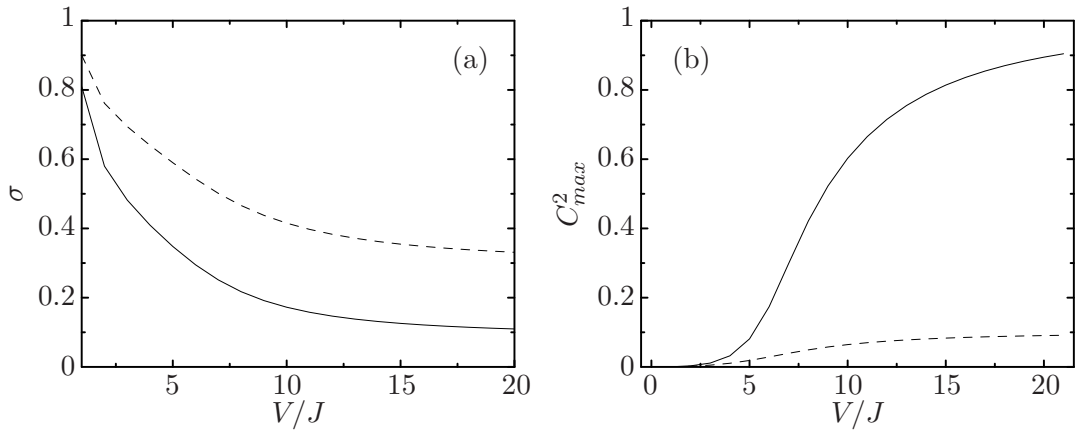

Figure 3.1: Plot of fluctuation (a) and maximum coefficient (b) as function of the interaction strength. The solid line shows results for commensurate filling (10-10-b) and the dashed line for incommensurate filling (10-9-b).

In the occupation number representation the fluctuation is closely related to the largest coefficient C^2_{max} in the expansion of the ground state (2.44) in terms of Fock states [19]

$$C^2_{max} \equiv \max(C^2_\alpha) \; . \tag{3.3}$$

Although it is not an experimental observable, we are able to analyse the behaviour of the largest coefficient under varying interaction strengths. Together the fluctuation and the largest coefficient give a first impression of the underlying structure of the ground state.

The numerical results of the fluctuations and the maximum coefficients for varying interaction strength V/J are shown in figure 3.1. For small interaction strengths, the system consists of a superposition of many Fock states with different occupation numbers at the individual lattice sites. Thus, there is no preferred Fock state and so C^2_{max} is small whereas fluctuations are large. With increasing interaction strength, the Fock states that have only a few atoms per site become energetically more favourable. Hence C^2_{max} increases and σ decreases. At large interaction strengths one might expect the commensurate filled system to be made up of only the Fock state that has one atom per lattice site. However, one has to consider that the hopping term of the Hubbard Hamiltonian (2.39) always connects this particular state with those that have one unoccupied and one doubly occupied site. This is why fluctuations are not fully suppressed at large interaction strength and remain finite even within the Mott-insulating phase.

The incommensurate filled system has 10 possibilities to place the hole and thus the value of C^2_{max} at high interaction strength is about 0.1 times the corresponding value of the commensurate filled system.

The major problems of our approach, i.e., calculating exact solutions of the Hamiltonian matrix, are finite size effects due to the consequential limitation in system sizes. To provide an insight into those effects we would have to perform our calculations for quantitative different but qualitative equal systems, e.g. 8-8-b, 10-10-b and 12-12-b for commensurate filling. This was done in [19]. The mean fluctuation barely suffers finite size effects because it is a local quantity that is evaluated at a single lattice site. Actually, its qualitative behaviour does not depend crucially on the filling rate as can be seen in figure 3.1. But for the same reason it does not provide much information about macroscopic properties of the system.

3.2 Condensate Fraction

A macroscopic observable is the condensate fraction, i.e., the fraction of particles that undergo Bose-Einstein condensation. In the standard picture, particles that participate in condensation are those that occupy the lowest single-particle state [14]. However, starting from the many-body groundstate (2.44), it is a non-trivial task to identify a possible Bose-Einstein condensate and extract the condensate wavefunction. But there is a possibility to obtain the single particle states and their occupation numbers.

Following the idea of Penrose, Onsager [24] and Yang [25], a Bose-Einstein condensate is present if one 'natural orbital' is macroscopically occupied. The corresponding eigenvalue gives the number of condensed particles N_c. The natural orbitals are the eigenvectors of the one-body density matrix $\rho^{(1)}$ (2.49). Thus, we can identify its largest eigenvalue with the number of condensed particles $\lambda_1 = N_c$. In terms of ODLRO this implies that if λ_1 is of the order of N, single particles form a basic group (section 2.7). One can show that in perfect lattices the natural orbitals satisfy Bloch's theorem and are therefore single-particle states [13]. Obviously the quasimomentum zero state is the lowest single-particle state. Figure 4.1 shows the numerical results of the eigenvectors of the one-body density matrix and reveal that they are indeed Bloch functions. In order to obtain a size-independent quantity, we define the condensate fraction [19]:

$$f_c \equiv N_c/N = \lambda_1/N \; . \tag{3.4}$$

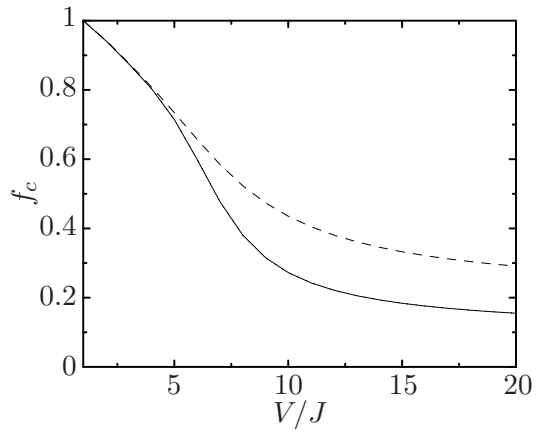

Figure 3.2: Plot of the condensate fraction as function of the interaction strength. The solid line corresponds to a commensurate 10-10-b system and the dashed line to an incommensurate 10-9-b system.

We immediately see that in finite systems there is always a finite condensate fraction. The normalisation of the one-body density matrix $\mathrm{Tr}\rho^{(1)}_{ll'} = N$ implies that there have to be eigenvalues larger or at least equal to N/I and therefore $f_c \geq 1/I$. This is a first indication, that dealing with macroscopic observables, we have to take care of finite size effects.

We saw in section 2.7 that the existence of a macroscopical eigenvalue of the one-body density matrix is equivalent to an intrinsic feature of a Bose-Einstein condensate, the existence of 'off-diagonal long range order' (2.60). That means

$$\rho^{(1)}_{ll'} \neq 0 \quad \text{for} \quad |l' - l| \to \infty \,. \tag{3.5}$$

In a demonstrative view this fact represents the delocalisation of a single particle within the condensate. The depletion of the condensate fraction as function of the interaction strength V/J is plotted in figure 3.2. The stronger the interaction is, the more the condensate fraction decreases, but as mentioned, remains finite even for large interaction strengths. The fringe visibility to be introduced next will point out that increasing interaction strength forces particles to successively occupy larger quasimomentum states. Hence, in the case of large interaction strengths, the occupation number of the lowest single particle state is always close to one. This leads to a higher condensate fraction for incommensurate filled systems.

3.3 Interference Pattern and Fringe Visibility

The following two observables are of particular interest, because they are directly experimental accessible. The matter-wave interference pattern is one of the most popular pictures (figure 3.3) when looking for informations about BEC on lattices. This 'borrowed' picture form Immanuel Bloch's group shows interference peaks of a released atom cloud. In the superfluid region, there are sharp interference patterns whereas they vanish in the Mott-insulating state. For detailed information we refer to [7]. In their experiment as well as in our calculations the depletion of the condensate is driven by particle-particle interactions and not by temperature so it is rather a quantum phase transition than a thermal phase transition. This is the definition of a *Mott*-insulating state.[1] Unfortunately, in an all-solid it is not possible to distinguish influences of electron-electron, electron-ion and other interactions leading to insulating states. But with the artificial crystals made of optical lattices one succeeded to examine pure Mott-insulator transitions.

After releasing the atoms from the lattice, the intensity of the matter-wave at a point x can be written as

$$\mathcal{I}(x) \equiv \left\langle \psi \,\middle|\, \hat{A}^\dagger(x)\,\hat{A}(x) \,\middle|\, \psi \right\rangle . \tag{3.6}$$

Since we are not interested in the spatial shape of the interference pattern the amplitude operator $\hat{A}(x)$ depends on the phase difference $\phi_l(x)$ between site l and the observation point x only,

$$\hat{A}(x) \equiv \frac{1}{\sqrt{I}} \sum_{l=1}^{I} e^{\mathbf{i}\,\phi_l(x)}\,\hat{a}_l \, . \tag{3.7}$$

Considering microscopic distances between the lattice sites and a macroscopic distance from the lattice to the observation point, we might neglect the phase shift coming from the spatial alignment of the lattice sites and assume a constant phase shift between adjacent sites $\delta = \phi_{l+1}(x) - \phi_l(x)$. Using this far-field limit, we obtain the following expression for the matter-wave interference pattern [20]:

$$\mathcal{I}(\delta) = \frac{1}{I} \sum_{l,l'=1}^{I} e^{\mathbf{i}(l-l')\delta} \left\langle \psi_0 \,\middle|\, \hat{a}_{l'}^\dagger \hat{a}_l \,\middle|\, \psi_0 \right\rangle = \frac{1}{I} \sum_{l,l'=1}^{I} e^{\mathbf{i}(l-l')\delta}\,\rho_{ll'}^{(1)} . \tag{3.8}$$

The latter expression is similar to the transformed one-body density matrix, i.e., the density matrix in quasimomentum representation (2.51). However, we scan continu-

[1] Sir Nevill Mott received the Nobel Prize (with P.W. Anderson and J.H. van Vleck) for his work on electron-electron properties in various materials in 1977.

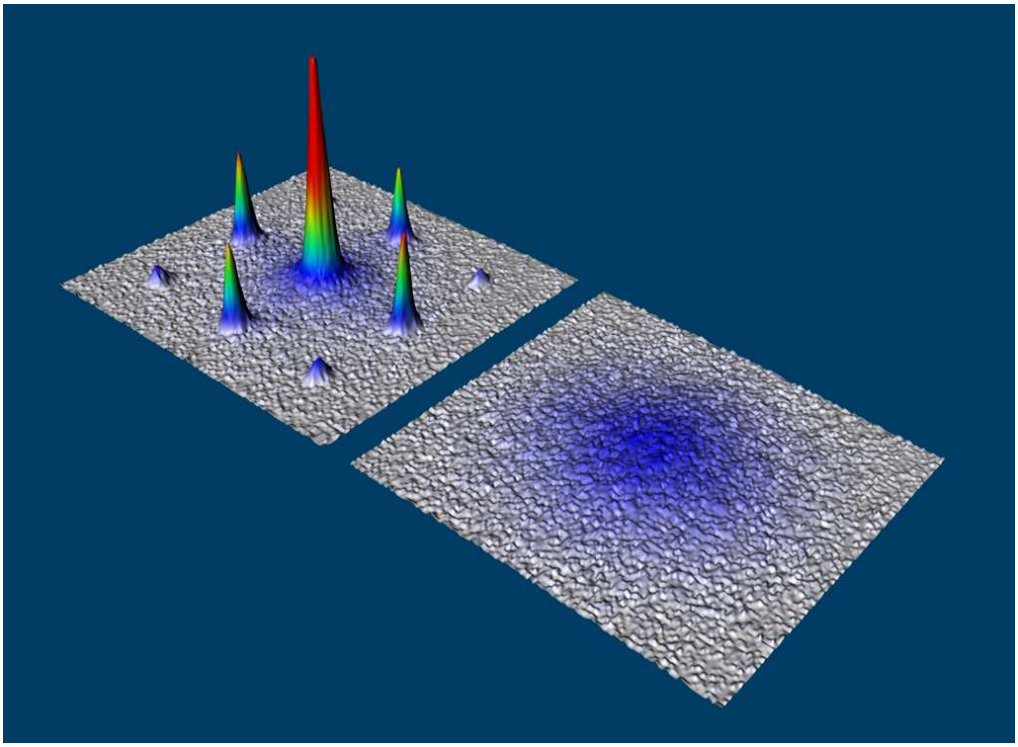

Figure 3.3: Experimental interference pattern of an atom cloud after release from the lattice, in the superfluid phase (left) and Mott phase (right). The picture was obtained by Immanuel Bloch's group [7]. Source: http://www.physik.uni-mainz.de/quantum/bec/gallery/mottadditional1.jpg

ously through the phase difference δ. For those δ that are integer multiples of $2\pi/I$, $\mathcal{I}(\delta)$ corresponds to the quasi-momentum occupation number n_q (2.58).

The numerical results presented in figure 3.4 show that an increasing interaction strength consequently leads to an increasing occupation of nonzero quasimomenta. This can be understood in terms of uncertainty. In the noninteracting regime we saw that the ground-state (2.44) is a superposition of many Fock states with different occupation numbers n_i at each site. The occupation number strongly fluctuates, hence particles are delocalised throughout the lattice. Therefore they are peaked in momentum space. Approaching larger interactions the fluctuation decreases and the occupation numbers become more and more fixed close to the mean occupation number n. Thus the wavefunction in momentum space broadens. In the limit of infinite interaction strength and for commensurate filling all quasimomenta are occupied with one particle and the interference pattern vanishes.

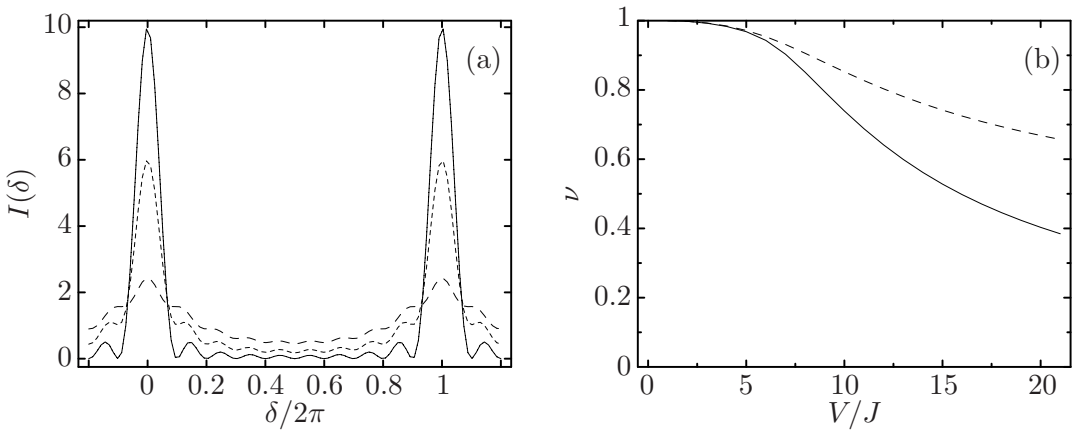

Figure 3.4: (a) shows the intensity of the matter wave interference pattern for $V/J = 0$ (solid), $V/J = 5$ (dotted) and $V/J = 10$ (dashed) as function of the phase difference for the commensurate filling. (b) shows the fringe visibility as function of the interaction strength for the commensurate filling (10-10-b, solid line) and the incommensurate filling (10-9-b, dashed line).

A directly related quantity is the visibility ν of the interference fringes, defined as [20]

$$\nu \equiv \frac{\mathcal{I}_{max} - \mathcal{I}_{min}}{\mathcal{I}_{max} + \mathcal{I}_{min}} \,. \tag{3.9}$$

Given that in our case $\mathcal{I}_{max} = \mathcal{I}(0)$ and $\mathcal{I}_{mim} = \mathcal{I}(\pi)$ – corresponding to $q = 0$ and $q = \pm 5$ respectively – the visibility provides information about the composition of occupation numbers in momentum space. As depicted in figure 3.4 it is one, if only the quasimomentum zero state is occupied and decreases with increasing interaction strength, i.e., successive occupation of higher quasimomentum states.

3.4 Superfluid Fraction

Another interesting quantity is the superfluid fraction f_s. It is an order parameter of the superfluid to Mott-insulator phase transition that was predicted by Fisher et al. in 1989 [26] and has been experimentally observed by Greiner et al. in 2002 [7]. The definition of superfluidity is directly related to flow properties. A demonstrative approach is the two fluid picture also used in the description of superfluid Helium (HeI and HeII). Consider we put a tube around our lattice and pull it in one direction, the normal fluid component is affected and follows the drag whereas the superfluid part stays at rest. In the frame of the moving tube, the superfluid part gains kinetic energy and via its velocity we

can derive an expression for the superfluid fraction. To induce the flow we could apply – for a given time Δt – a linear external potential $\hat{V} = F\ \hat{x}$ to our groundstate to generate a directed momentum p. This can be written as a unitary transformation of our groundstate $\mid \psi \rangle$ to a Galilei boosted $\mid \psi \rangle_{TW}$ with the position operator $\hat{x}$ as the generator

$$\begin{aligned} \mid \psi \rangle_{TW} &\equiv e^{\mathbf{i}/\hbar p\,\hat{x}} \mid \psi \rangle & (3.10)\\ &= e^{\mathbf{i}/\hbar\,\vartheta(\hat{x})} \mid \psi \rangle\,. & (3.11) \end{aligned}$$

We see that a velocity field $v = \frac{\hbar}{m}\nabla\vartheta(x)$ might be obtained by a spatial variation of the phase [14],[27]. Technically we can generate this phase variation by imposing so called 'twisted boundary conditions'. The wavefunction gains a phase Θ each time a particle runs once through the lattice

$$\langle\, x_1, \ldots, x_k + L, \ldots, x_N \mid \psi_\Theta \,\rangle = e^{\mathbf{i}\Theta} \langle\, x_1, \ldots, x_k, \ldots, x_N \mid \psi_\Theta \,\rangle\,. \tag{3.12}$$

Note that the boundary conditions are no longer periodic. A phase variation of the form

$$\vartheta(x) = \Theta/L\,x \tag{3.13}$$

fulfils the demand (3.12). The Schroedinger equation of the twisted groundstate reads:

$$\hat{H}_\Theta \mid \psi_\Theta \rangle = E_\Theta \mid \psi_\Theta \rangle\,. \tag{3.14}$$

We can write down an expression for the kinetic energy T_s of the superfluid part with mass M_s in which E_0 is the energy of the system without the flow

$$T_s = E_\Theta - E_0 = \frac{1}{2}M_s v^2 = \frac{1}{2}M_s\left(\frac{\hbar}{m}\nabla\vartheta(x)\right)^2 = \frac{1}{2}M_s\left(\frac{\hbar}{m}\frac{\Theta}{L}\right)^2\,. \tag{3.15}$$

There is a restriction to the magnitude of Θ: it has to be sufficiently small so that the flow is not able to excite higher states. We will come back to this point later. Introducing the superfluid fraction $\tilde{f}_s$ as the ratio of the superfluid mass M_s to the total mass $M_{tot} = N\,m$, we can cast it into the form

$$\tilde{f}_s \equiv \frac{M_s}{M_{tot}} = \frac{2mL^2}{\hbar^2 N}\frac{E_\Theta - E_0}{\Theta^2} = \frac{2ma^2}{\hbar^2}\frac{I^2(E_\Theta - E_0)}{N\Theta^2}\,. \tag{3.16}$$

Now we have to translate the prefactor of the latter expression into the language of the Hubbard model. We will motivate that this prefactor is nearly the tunnelling energy of the Hubbard Hamiltonian. Comparing the kinetic energy of a free particle with the kinetic energy of a particle in a periodic lattice, we saw in section 2.2, that the

dispersion relation is no longer parabolic (figure 2.1). For small momenta, one can compensate this with an effectice mass term that simply broadens the shape at the centre of the parabola. Therefore the kinetic energy in the lattice is approximately of the form $E_{latt}(k) = \hbar^2 k^2/2m^\star$. The expectation value of this energy can be identified with the tunnelling energy $J = \hbar^2/(2a^2 m^\star)$ (2.39). So we obtain an expression for the superfluid fraction

$$\tilde{f}_s = \frac{m}{m^\star}\frac{I^2}{NJ}\frac{E_\Theta - E_0}{\Theta^2} \equiv \frac{m}{m^\star} f_s \,. \tag{3.17}$$

The reader that is not satisfied with the latter line of arguments should notice that the coefficient $I^2/(NJ)$ simply serves the purpose of normalising the superfluid fraction. The factor $m/m^\star$ reflects the depletion of the superfluid flow by the lattice itself. In our description we have no access to this effect. Thus, the superfluid fraction f_s we are going to discuss accounts for effects of the two-body interaction only [20]

$$f_s = \frac{I^2}{NJ}\frac{E_\Theta - E_0}{\Theta^2} \,. \tag{3.18}$$

We now have to show how to describe the flow in terms of the Hubbard model. We can map the phase variation (3.13) to the Hamiltonian (2.42) by means of the unitary many-particle operator

$$\hat{U} \equiv \bigotimes_{n=1}^{N} e^{\mathbf{i}\,\frac{\Theta\,\hat{x}}{L}} \quad , \quad \big|\, \psi_\Theta \,\big\rangle \equiv \hat{U} \,\big|\, \psi \,\big\rangle \,. \tag{3.19}$$

The phase variation only affects the hopping part because it commutes with the occupation number operators $[\hat{U}, \hat{n}_i] = 0$. This yields the twisted Hamiltonian,

$$\hat{H}_\Theta = \hat{U}^\dagger \hat{H}_0 \hat{U} = -J\sum_{i=1}^{I}(e^{-\mathbf{i}\frac{\Theta}{I}}\hat{a}_{i+1}^\dagger \hat{a}_i + \hat{a}_i^\dagger \hat{a}_{i+1} e^{\mathbf{i}\frac{\Theta}{I}}) + \frac{V}{2}\sum_{i=1}^{I}\hat{n}_i(\hat{n}_i - 1) \tag{3.20}$$

where a is the lattice spacing thus $L = a\,I$. We used:

$$\begin{aligned} \hat{U}^\dagger\,\hat{a}_{i+1}^\dagger\,\hat{1}\,\hat{a}_i\,\hat{U} &= \hat{U}^\dagger\,\hat{a}_{i+1}^\dagger\,\hat{U}\,\hat{U}^\dagger\,\hat{a}_i\,\hat{U} \\ &= e^{-\mathbf{i}\frac{\Theta a(i+1)}{L}}\,\hat{a}_{i+1}^\dagger\,\hat{a}_i\,e^{\mathbf{i}\frac{\Theta a i}{L}} \\ &= e^{-\mathbf{i}\frac{\Theta a}{L}}\,\hat{a}_{i+1}^\dagger\,\hat{a}_i \,, \end{aligned} \tag{3.21}$$

so every particle gains a constant phase during each tunnel process. The factor $e^{-\mathbf{i}\frac{\Theta a}{L}}$ is called Peierls phase factor.

Note that the second equality sign in equation (3.20) is only correct in the case of

boxed boundary conditions or a lattice of infinite length. If we use periodic boundary conditions, the Peierls phase factor for hopping over these boundaries has to be

$$\begin{aligned} \hat{U}^\dagger \, \hat{a}_I^\dagger \, \hat{1} \, \hat{a}_1 \, \hat{U} &= \hat{U}^\dagger \, \hat{a}_I^\dagger \, \hat{U} \, \hat{U}^\dagger \, \hat{a}_1 \, \hat{U} \\ &= e^{-\mathbf{i}\frac{\Theta a(I)}{L}} \, \hat{a}_I^\dagger \, \hat{a}_1 \, e^{\mathbf{i}\frac{\Theta a}{L}} \\ &= e^{-\mathbf{i}\frac{\Theta a(I-1)}{L}} \, \hat{a}_I^\dagger \, \hat{a}_1 \end{aligned} \tag{3.22}$$

in order to preserve the unitarity of U. Without this violation of unitarity, H_Θ would have the same eigenspectrum as H_0 because unitary transformations do not change eigenspectra. Thus, neglecting (3.22) and applying a constant Periels phase factor as done in (3.20) even at the boundaries leads to the net phase shift $\mathbf{i}\Theta$ we claimed in (3.12). This 'twist' of the phase at the boundary is the reason why one calls this procedure an imposing of 'twisted boundary conditions'.

As already mentioned we have to assure that the imposed velocity field is small enough to prevent excitations of the system. Figure 3.5 shows how the energy of the twisted commensurate system depends on the twist angle Θ. We see that for $V/J = 0$ the kinetic energy is exactly parabolic – $T_s \propto \Theta^2$ – but for $\Theta \approx \pi$ a level crossing between the groundstate and the first excited state of the twisted system takes place. Interaction strengths larger than zero lead to a level repulsion that deforms the parabola. This effect increases with raising interaction strengths. In the incommensurate system there is no level repulsion, as depicted in figure 3.6. Since we want the superfluid fraction f_s to be independent of Θ and we also want to obtain valid results for strong interactions, we have to perform our calculations at a small value of Θ. We choose $\Theta = 0.1$, for which the deviation from the parabola is negligible for all interaction strengths.

The numerical results depicted in figure 3.7 show a rapid decrease of the superfluid fraction f_s at $3 < V/J < 7$. This is in good agreement with the extrapolated transition point $V/J \approx 4.65$ based upon Monte Carlo [28] and coupling expansion methods [29].

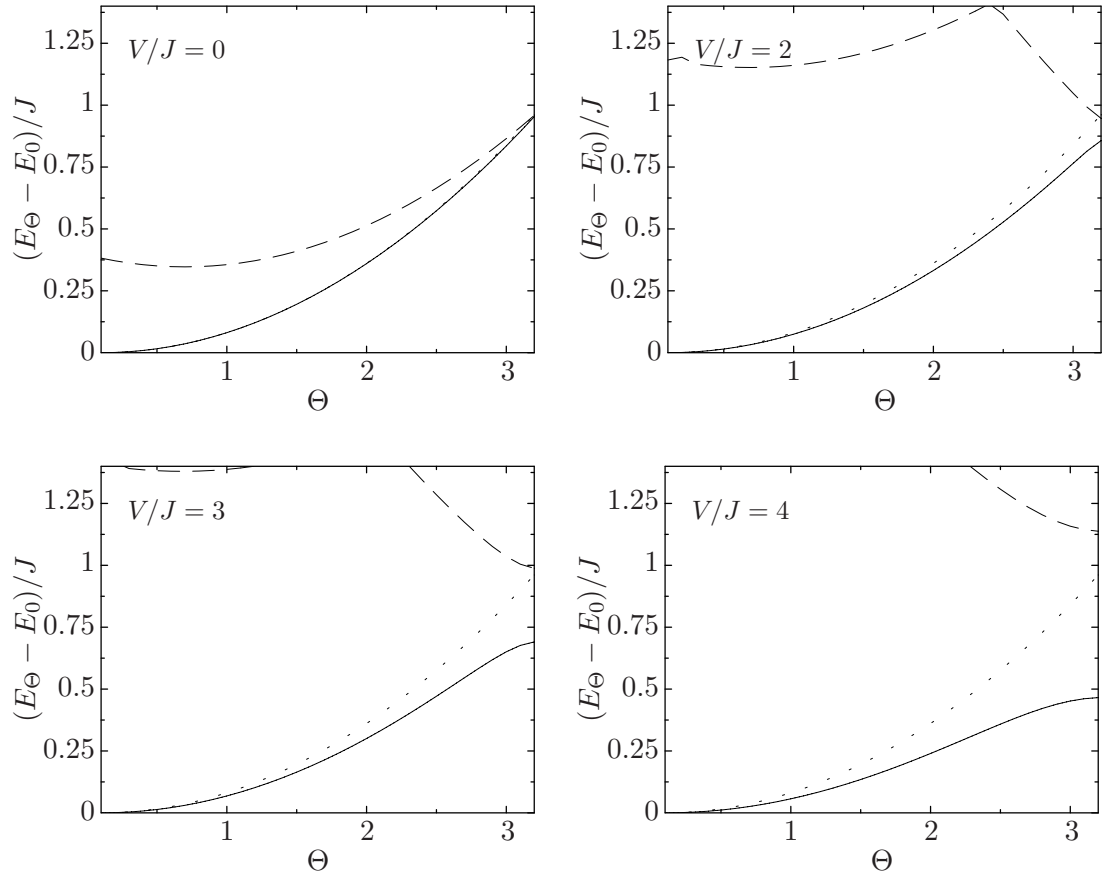

Figure 3.5: The solid lines show the difference of groundstate energies of the twisted and the untwisted Hamiltonian for the commensurate system (10-10-b). The dashed lines show the difference of the first excited state of the twisted and the groundstate of the untwisted Hamiltonian. The dotted line is the kinetic energy of a free particle $E(\Theta) \propto \Theta^2$. Top left to bottom right $V/J = 0$,$V/J = 2$, $V/J = 3$, and $V/J = 4$.

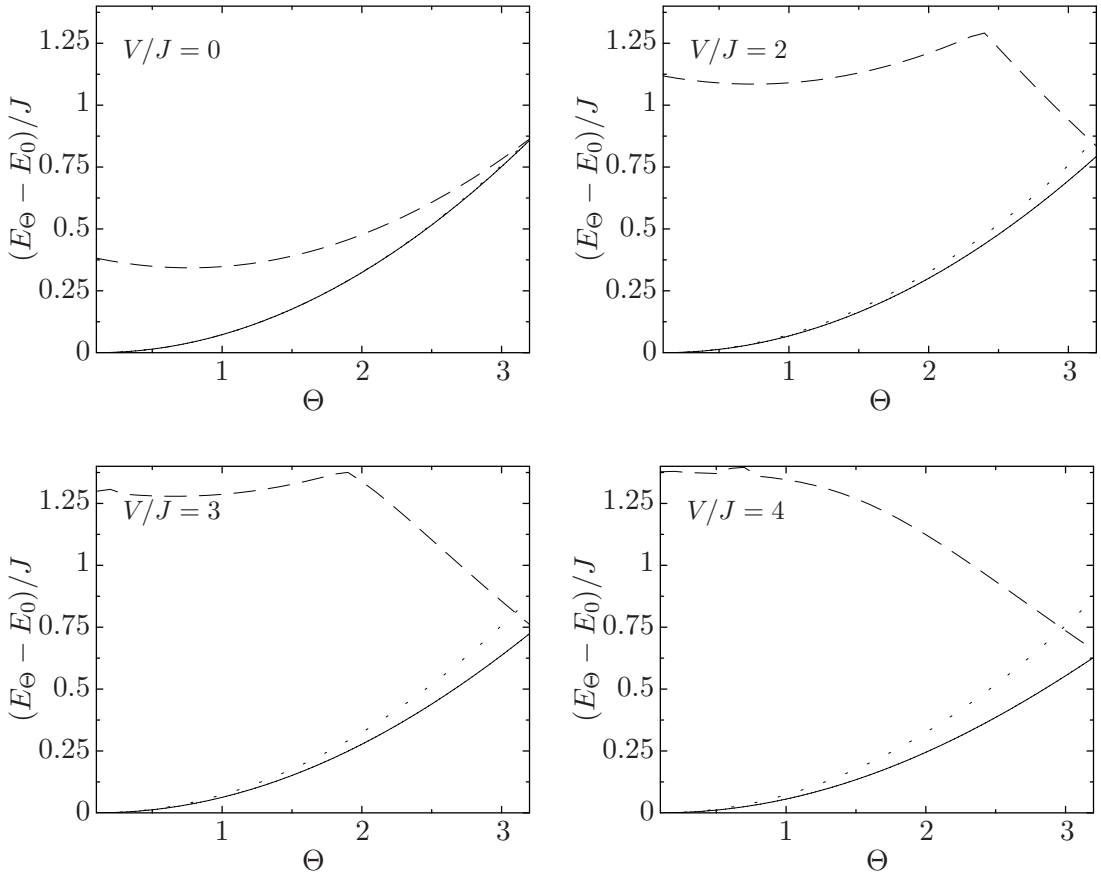

Figure 3.6: The solid lines show the difference of groundstate energies of the twisted and the untwisted Hamiltonian for an incommensurate system (10-9-b). The dashed lines show the difference of the first excited state of the twisted and the groundstate of the untwisted Hamiltonian. The dotted line is the kinetic energy of a free particle $E(\Theta) =\propto \Theta^2$. Top left to bottom right $V/J = 0$, $V/J = 2$, $V/J = 3$, and $V/J = 4$.

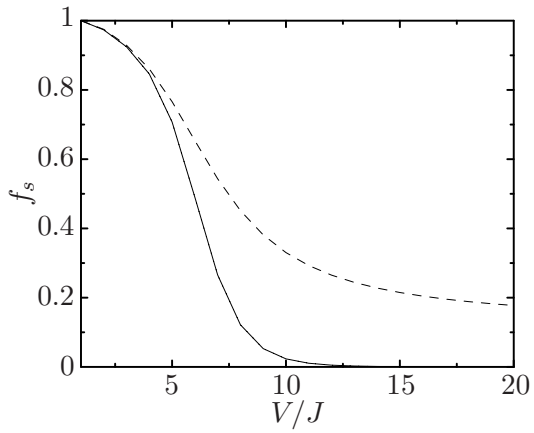

Figure 3.7: The plot shows the superfluid fraction as function of the interaction strength. Commensurate filling (10-10-b, solid line) and incommensurate filling (10-9-b, dashed line). Extrapolation to the thermodynamic limit based upon Monte Carlo and coupling expansion calculations predict a Mott-insulator transition at $V/J \approx 4.65$ for commensurate systems. In accordance with band theory, there is no insulating phase in the incommensurate system.

A very important feature coming to light when comparing the superfluid fraction with the fringe visibility is that although the system is in a Mott-insulating phase for $V/J > 7$ the interference fringes are still visible. As a conclusion we see that superfluidity has to be clearly distinguished from condensation. A famous example is Helium II which is 100% superfluid whereas only 10% participate in the formation of a Bose-Einstein condensate.

3.5 Fringe Visibility & External Trapping Potential

Inspired by recent experiments in the group of Immanuel Bloch we examined the behaviour of the fringe visibility in the presence of an external trapping potential. Their measured fringe visibility shows small kinks, which are attributed to a rearrangement of particles due to the harmonic trapping potential [30]. The Hamiltonian (2.42) is now supplemented by an additional single-particle potential with on-site energies ϵ_i as discussed in section 2.6

$$\hat{H}_0 = -J \sum_{l=1}^{I} (\hat{a}_{l+1}^{\dagger} \hat{a}_l + h.a.) + \frac{1}{2} V \sum_{l=1}^{I} \hat{n}_l (\hat{n}_l - 1) + \sum_{l=1}^{I} \epsilon_l \, \hat{n}_l \, . \tag{3.23}$$

The trapping potential is harmonic and centred at the middle of the lattice. The on-site energies are given by

$$\epsilon_l = \left(\frac{l-1}{I-1} - 0.5 \right)^2 \cdot 4 \cdot \Delta \, , \tag{3.24}$$

where Δ is the potential energy at the boundary of the lattice.

Our numerical results for a commensurate system consisting of $N = 12$ bosons on $I = 12$ lattice sites that has a basis dimension of $D = 1352078$ Fock states and an incommensurate system ($I = 12$, $N = 11$, $D = 352716$), are calculated at $\Delta/J = 20$ and $\Delta/J = 30$. The results are shown in figure 3.8. The dashed lines show the fringe visibility without external trapping potential, i.e., $\Delta/J = 0$. There are several small bumps due to rearrangements of the system. The bigger ones at $V/J \approx 12$, $\Delta/J = 20$ and $V/J \approx 17$, $\Delta/J = 30$, respectively, are caused by a rearrangement at the centre of the trap from a Mott like state with $n = 2$ to a state with $n < 2$. During those 'transitions' the fluctuations and therefore the visibility increase as shown in figures 3.10 and 3.12. This effect might not be accessible by experiments. Because of the much larger number of lattice sites and particles, this will happen rather continously every time the occupation numbers change and all the bumps will overlap resulting in a net upward shift of the entire curve. This changes at the step seen at $V/J \approx 22$, $\Delta/J = 20$ and $V/J \approx 33$, $\Delta/J = 30$. There the interaction energy is sufficiently strong to push particles to the outer rim of the lattice. From the mean occupation number (figures 3.9 and 3.11) and the fluctuation (figures 3.10 and 3.12) we see that this is the genuine transition to a homogeneous Mott phase with $n_l = 1$ and $\sigma_l \approx 0 \; \forall \, l$ for the commensurate system. The incommensurate system shows an occupation number 0.5 at the rims due to the odd number of particles – for this reason the fluctuation is large there. No further rearrangement is possible for increasing V/J. This transition is unique and depends neither on the lattice size nor on the dimension and should be therefore experimentally observable. Incommensurate systems behave almost in the same manner. They just show a slower decline of the fringe visibility for large values of V/J. This is due to the fact that the fluctuations do not vanish as much as in a Mott state. In an overfilled system the residual particles can slide upon those that form the Mott state, in the underfilled case there is still space left for particles to move even at large interaction strengths (e.g. the large fluctuations at the rims depicted in figure 3.12).

In an experimental setup, commensurate and incommensurate filling is not an appropriate characterisation of the system because the atoms will never 'see' the whole lattice.

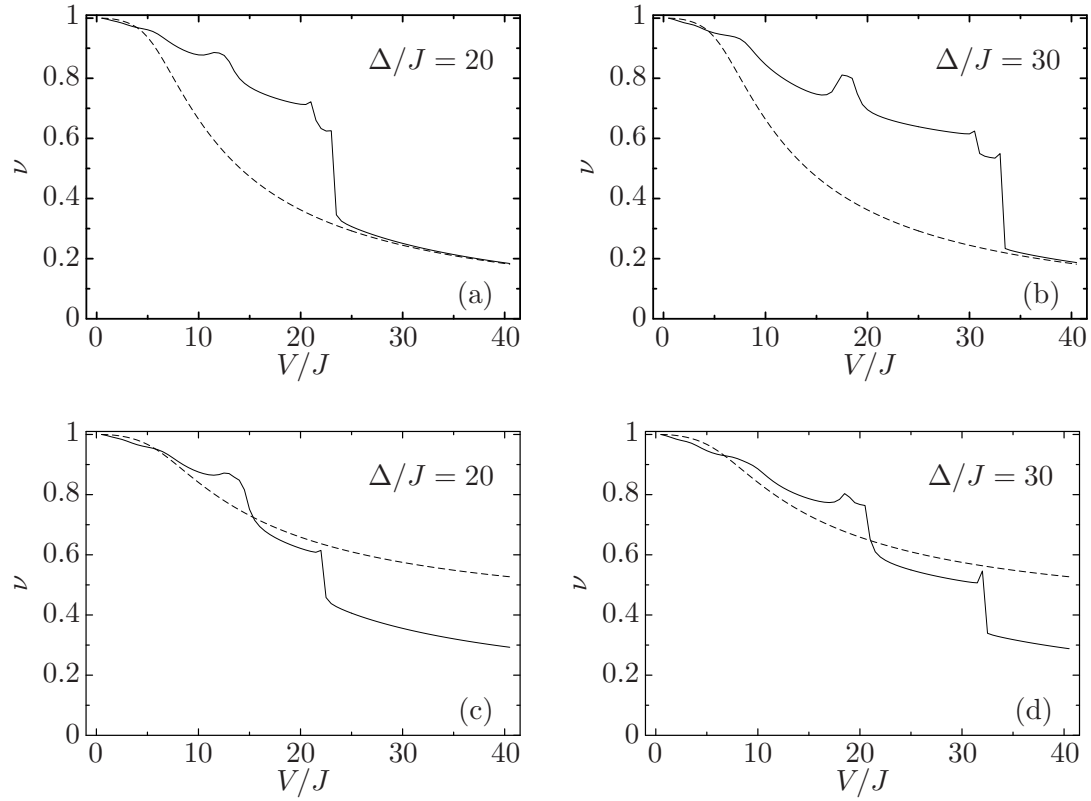

Figure 3.8: Fringe visibility as function of the interaction strength. The solid line depicts results with an external trapping potential and the dashed line without an external trapping potential. Panels (a), (b) present results for the system with commensurate filling (10-10-b) and panels (c), (d) for the incommensurate filled systems (10-9-b).

Their sole confinement is the trapping potential.

Note that during the definition of the tunnelling energy J (2.39) we neglected the influence of the external trapping potential $V_T(x)$ due to its small gradient on a scale of the distance between the lattice sites. Here we actually used a significant gradient of the trapping potential and thus it is an approximation to neglect the dependence of the tunnelling energy on the index of the lattice site $J_l \approx J$.

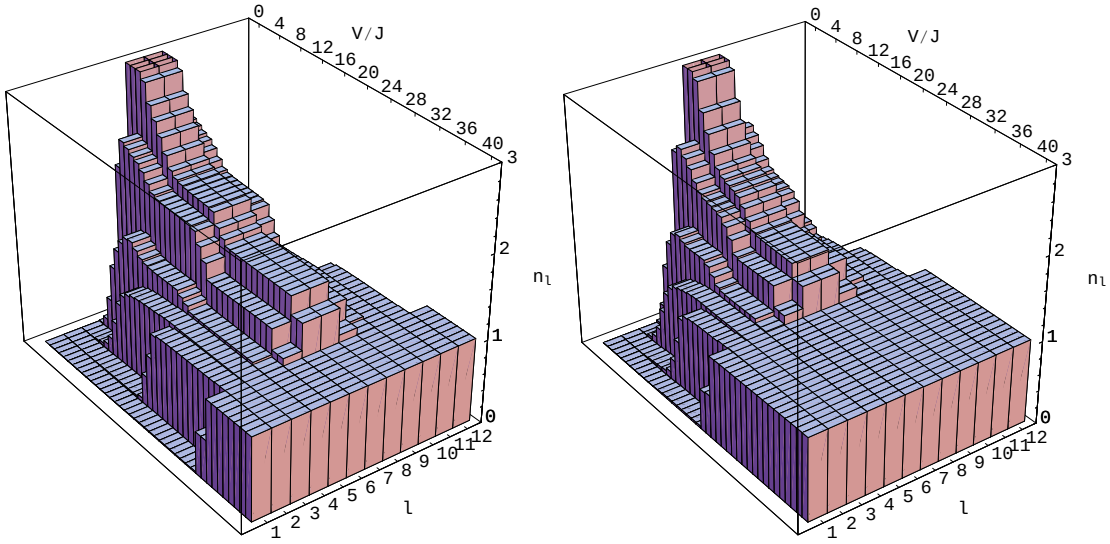

Figure 3.9: Taking an external trapping potential into account, the mean occupation number depends on the interaction strength and the number of lattice site l. Left panel: $\Delta/J = 20$, right panel: $\Delta/J = 30$. Both calculations were done for a commensurate 12-12-b system.

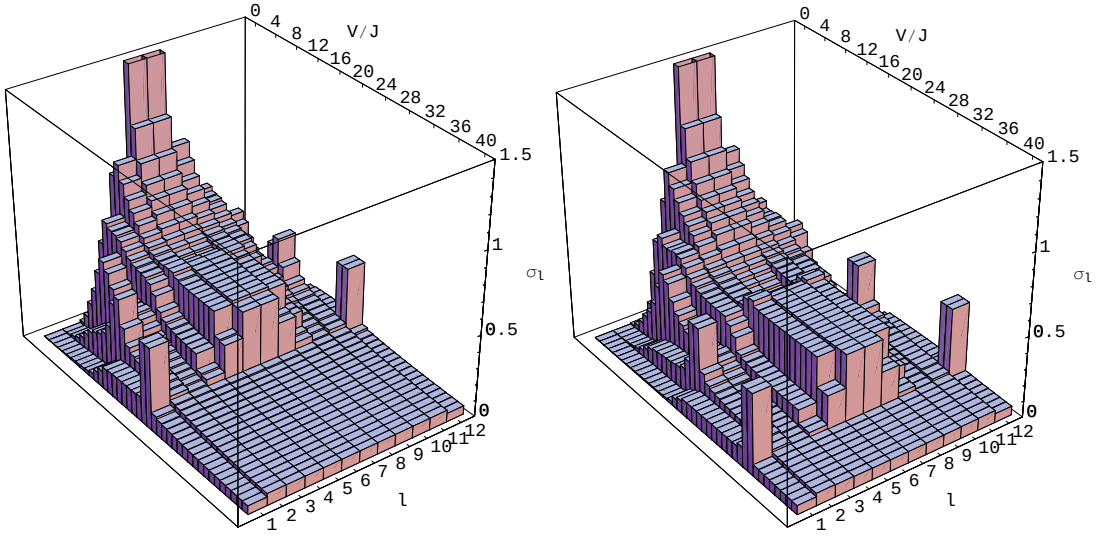

Figure 3.10: cf. figure 3.9. The plot shows the fluctuations as function of the lattice site and the interaction strength. Left panel: $\Delta/J = 20$, right panel: $\Delta/J = 30$. Both calculations were done for a commensurate 12-12-b system.

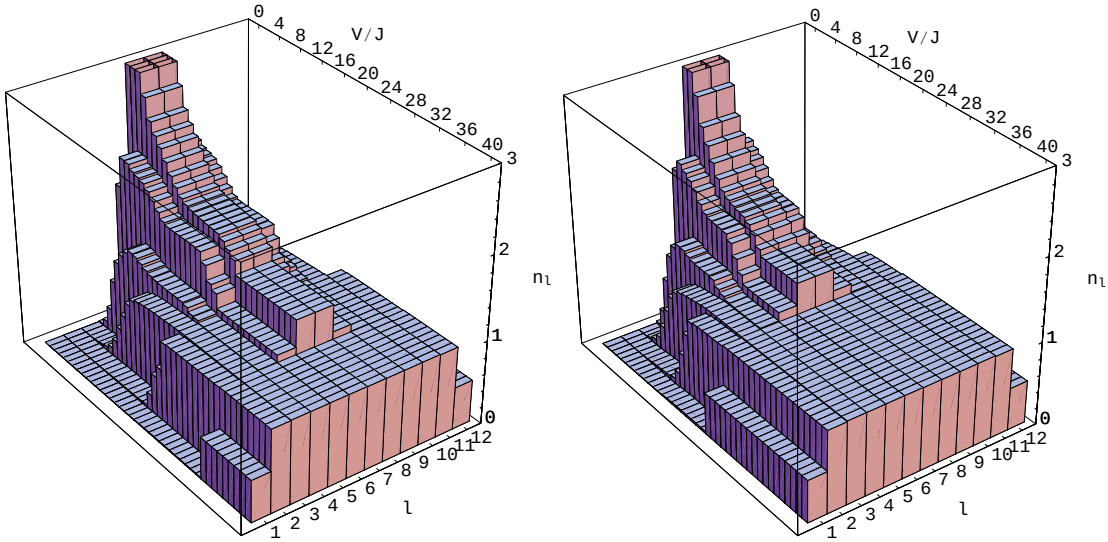

Figure 3.11: cf. figure 3.9. The mean occupation numbers as function of the interaction strength and the lattice site. Left panel: $\Delta/J = 20$, right panel: $\Delta/J = 30$. Both calculations were done for an incommensurate 12-11-b system.

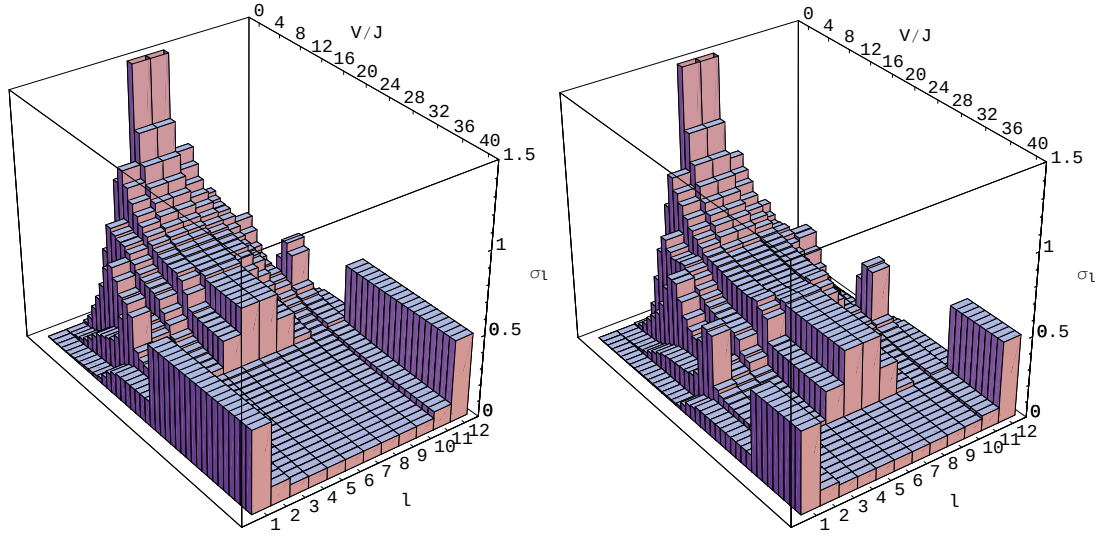

Figure 3.12: cf. figure 3.9. The plot shows the fluctuations as function of the lattice site and the interaction strength. Left panel: $\Delta/J = 20$, right panel: $\Delta/J = 30$. Both calculations were done for an incommensurate 12-11-b system. The large fluctuation at the rim are due to the odd number of particles.

Chapter 4

Two-Component Fermi Gases

4.1 Fermi-Fermi Hubbard Model

Formally, we extend the Bose Hubbard Hamiltonian to the Fermi-Fermi Hubbard Hamiltonian by adding another hopping operator for a second species and an interaction operator between the two species. Furthermore we impose anticommutation relations for the fermionic creation and annihilation operators. Due to the restriction to the first energy band, there is no on-site interaction within the species. The different species a and b may be considered as fermionic atoms of the same type with different spins (up and down) or as different types of fermionic atoms. Assuming the same tunnelling matrix element J for both species, the Fermi-Fermi Hubbard Hamiltonian reads:

$$\hat{H} = -J \sum_{l=1}^{I} \left(\hat{a}_{l+1}^{\dagger} \hat{a}_l + \hat{b}_{l+1}^{\dagger} \hat{b}_l + \ h.a. \right) + V_{ab} \sum_{l=1}^{I} \hat{n}_l^{(a)} \, \hat{n}_l^{(b)} \ . \tag{4.1}$$

The groundstate is a sum over tensor products of the two species' Fock states

$$\mid \psi \rangle \equiv \sum_{\alpha=1}^{D_a} \sum_{\beta=1}^{D_b} C_{\alpha\beta} \mid \{n_1^{(a)}, \ldots, n_I^{(a)}\}_{\alpha} \rangle \otimes \mid \{n_1^{(b)}, \ldots, n_I^{(b)}\}_{\beta} \rangle \ . \tag{4.2}$$

Again the sum runs over all possible Fock states and the coefficients $C_{\alpha\beta}$ are obtained from the diagonalisation of the Hamilton matrix (2.45).

The operators $\hat{a}_l, \hat{a}_l^\dagger, \hat{n}_l^{(a)}$ and $\hat{b}_l, \hat{b}_l^\dagger, \hat{n}_l^{(b)}$ act on their respective sub space

$$\begin{aligned} \hat{a}_l \mid \psi \rangle &\equiv \hat{a}_l \otimes \hat{1} \mid \psi \rangle \\ \hat{b}_l \mid \psi \rangle &\equiv \hat{1} \otimes \hat{b}_l \mid \psi \rangle \\ \hat{n}_l^{(a)} &\equiv \hat{n}_l \otimes \hat{1} \mid \psi \rangle \\ \hat{n}_l^{(b)} &\equiv \hat{1} \otimes \hat{n}_l \mid \psi \rangle \,. \end{aligned}$$

In the following all operators are supposed to act in the similar manner. First of all we test the groundstate obtained by the numerical solution of the eigenproblem. To this end we diagonalise the one-body density matrix. For a translationally invariant lattice the eigenvectors – the so called 'natural orbitals' – correspond to Bloch functions and the eigenvalues to their occupation numbers n_q [13]. To check those properties we fit a function $f(x) = A \sin(\frac{2\pi}{I} q x + \phi)$ to the eigenvectors. The fit parameters are A, ϕ and q. The result is shown in figure 4.1. The dots show the values obtained from the eigenvectors of the one-body density matrix and the lines the fitted function. Note that there are two one-body density matrices now, one for species a and one for species b. For all systems discussed here they will be equal and we discuss exemplarily one of them. Only integer values of q appear and the occupation numbers in momentum space, depicted in figure 4.2, fulfil Pauli's principle: $0 \leq n_q \leq 1$. This is in agreement with the expectation and has been tested for different interaction strengths and for all system types. Hence, we can be sure our implementation works and yields the results expected.

After we finished the implementation and examined the results for the first time we were surprised by the fact that the first Bloch band ($q = 0$) was occupied with more than one particle, i.e., $n_{q=0} > 1$. But fermions should obey Pauli's principle in coordinate as well as in momentum space. It took us several weeks until we realised that during the implementation of the Fermi-Fermi Hubbard Hamiltonian (4.1) we forgot about the crucial fact that fermionic wavefunctions have to be antisymmetric or in other words the anticommutation relations, have to be imposed. We never thought about sorting the creation operators that create a particular Fock state out of the vacuum (2.26) when implementing the Bose Hubbard Hamiltonian. But when dealing with fermions this is absolutely necessary. One can easily see that for an even number of fermions hopping over the periodic boundary generates a minus sign. But that would mean applying antiperiodic boundary conditions. We will come back to that point at the end of the chapter. However, for any calculation of density matrices the anticommutator relations are of major importance as we saw in section 2.4.

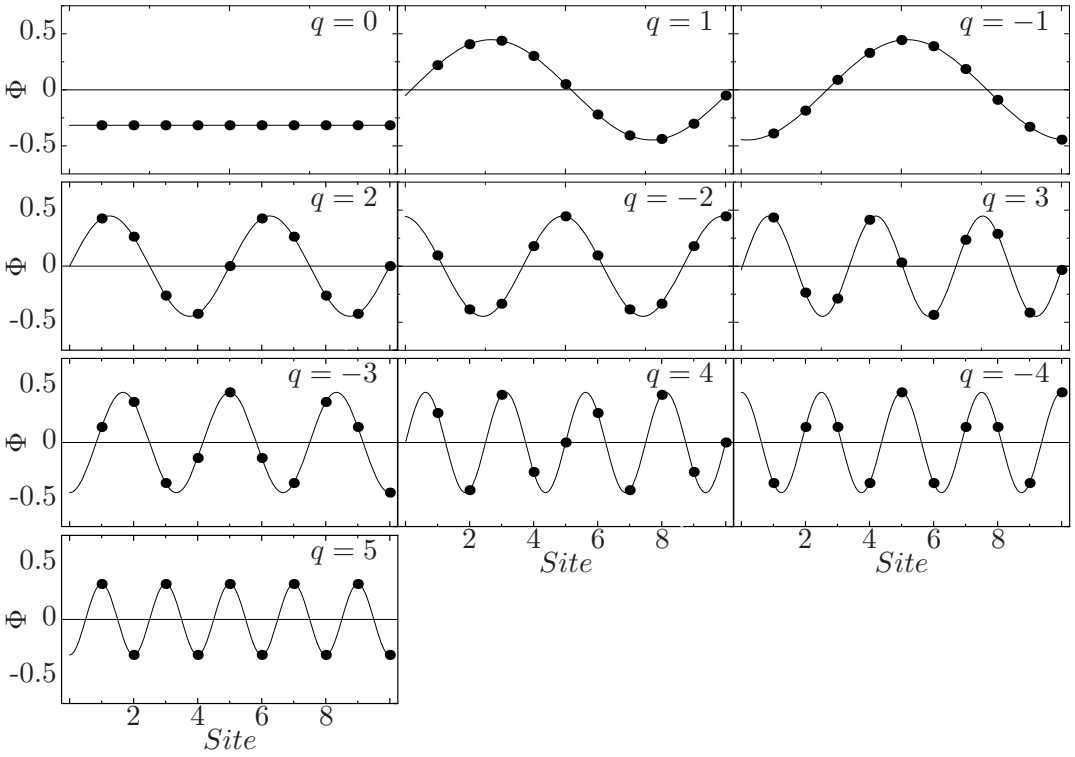

Figure 4.1: To test the numerics, the natural orbitals of a 10-5-5-ff system are fitted to Bloch functions at $V_{ab}/J = 5$. Top left to bottom right: $q = 0, 1, -1, 2, -2, 3, -3, 4, -4, 5$. The dots are the computed values of the eigenvectors, the lines are the fitted functions.

We will examine two different systems in the following: (*i*) A system labelled '10-5-5-ff' with $I = 10$ lattice sites and $N_a = N_b = 5$, i.e., half-filling of the lattice. (*ii*) A system termed '12-5-5-ff' with $I = 12$ lattice sites and $N_a = N_b = 5$.

The simple observables, like the mean occupation number, number fluctuations and largest coefficient do not provide useful probes for fermionic systems. Again it is obvious that the mean occupation number n_l has to be constant at all lattice sites due to the periodic boundary conditions and the absence of an external trapping potential. The fluctuations σ_l^2 always have to be independent of l, but furthermore they are constant for all interaction strengths V_{ab}/J.

$$\sigma^2 \equiv \sigma_l = \left\langle \psi \,\middle|\, \hat{n}_l^2 \,\middle|\, \psi \right\rangle - \left\langle \psi \,\middle|\, \hat{n}_l \,\middle|\, \psi \right\rangle^2 = \text{const} = N/I - (N/I)^2 \tag{4.3}$$

This is obvious because every time the occupation number operator $\hat{n}_l$ acts on a particular Fock state, the l-th lattice site is either occupied and returns one or unoccupied

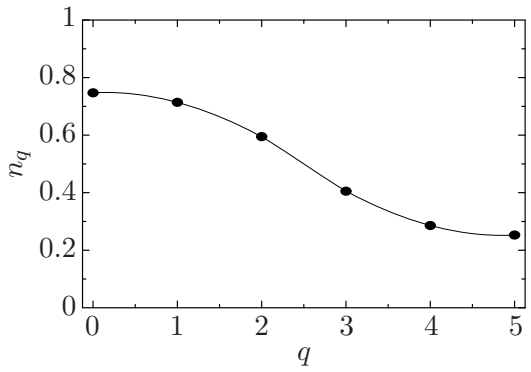

Figure 4.2: The plot shows the occupation numbers of quasimomentum eigenstates for $V_{ab}/J = 5$. Because of the Pauli principle they have to be $0 \leq n_q \leq 1$. The dots are computed values, the line should guide the eye.

and returns zero. Hence, for fermions this operator is idempotent $\hat{n}_l^2 = \hat{n}_l$ and leads to equation (4.3).

The maximum coefficient C_{max}^2 is also deprived of his nice features. Again it is small at small interaction strengths where all possible states contribute but there is no unique Mott state with one atom per site as in the commensurate bosonic system. So we have to make a little more effort to disclose some interesting features of fermions on periodic lattices.

4.2 Pair-Coherence Function

The Pauli principle forbids a multiple occupation of a lattice site with atoms of the same kind and thus an on-site pairing within the species. Keeping in mind the discussion about ODLRO and macroscopical eigenvalues in section 2.7, we see that while dealing with fermionic systems one-body density matrices are no longer an appropriate tool to obtain nontrivial results. The next deductive step is to consult two-body density matrices.

As a first measure for two-particle properties we define the pair-coherence function $S(\delta)$. We use those matrix elements that annihilate a pair of different particles at lattice site $1 + \delta$ and create it again at site 1. We subtract the one-body quantities to get rid of the one-body density information, and to assure that if particles are uncorrelated – i.e., the

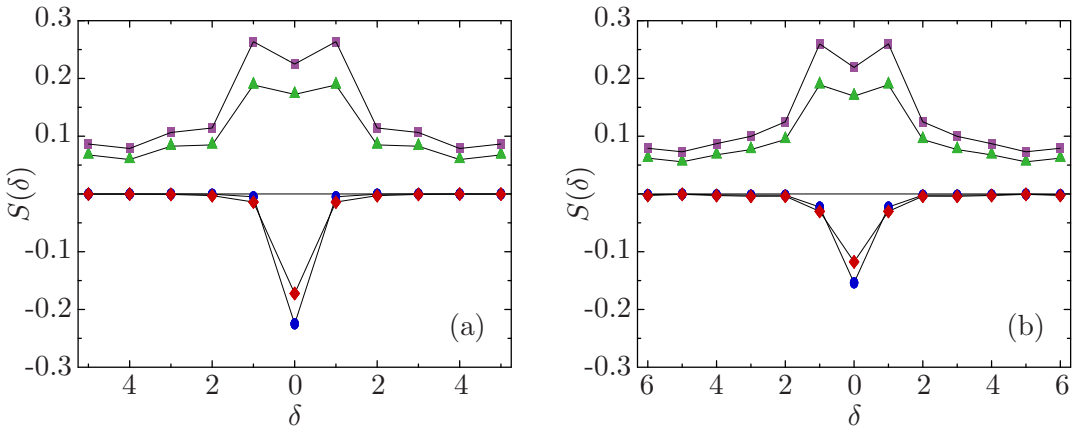

Figure 4.3: Pair-coherence function $S(\delta)$ as function of the lattice distance δ. The dots are the computed values. (a) for the 10-5-5-ff system and (b) for the 12-5-5-ff system. Circles correspond to $V_{ab}/J = 10$, diamonds to $V_{ab}/J = 5$, triangles to $V_{ab}/J = -5$ and squares to $V_{ab}/J = -10$. For attractive interactions, pairs show a long-range pair-coherence.

state is a Slater determinant – the pair-coherence function vanishes. Note that exchange terms $\langle\ \psi\ |\ \hat{a}_1^\dagger \hat{b}_{1+\delta}\ |\ \psi\ \rangle\ \langle\ \psi\ |\ \hat{b}_1^\dagger \hat{a}_{1+\delta}\ |\ \psi\ \rangle$ are zero due to the fixed particle numbers within each species. Thus, the pair-coherence function is defined as:

$$\begin{aligned} S(\delta) \quad \equiv \quad & \langle\ \psi\ |\ \hat{a}_1^\dagger \hat{b}_1^\dagger \hat{b}_{1+\delta} \hat{a}_{1+\delta}\ |\ \psi\ \rangle \\ & - \langle\ \psi\ |\ \hat{a}_1^\dagger \hat{a}_{1+\delta}\ |\ \psi\ \rangle\ \langle\ \psi\ |\ \hat{b}_1^\dagger \hat{b}_{1+\delta}\ |\ \psi\ \rangle\ . \end{aligned} \tag{4.4}$$

The numerical results are shown in figure 4.3. The symbols show the computed values, the lines are plotted to guide the eye.

For repulsive interactions $V_{ab}/J > 0$ we observe an anti-correlation at the same lattice site ($\delta = 0$) for both systems. This is not suprising, because if particles repel each other, it is energetically unfavourable to occupy the same lattice site. There is no correlation for distances δ larger than one. Keeping in mind that the Hamiltonian connects adjacent lattice sites, we can understand why the correlation extends at least to one site. In the region of attractive interactions it is again easy to understand, why there is strong correlation of pairs at the same lattice site, i.e., $\delta = 0$. If particles attract eachother, they want to occupy the same lattice site. Again one can see the correlation coming from the hopping term at $\delta = 1$. The non-trivial result for attractive interactions, is the long-range pair-coherence exhibited by fermion pairs, as indicated by the finite value of $S(\delta)$ for large distances δ. This means that pairs are delocalised in coordinate space similar

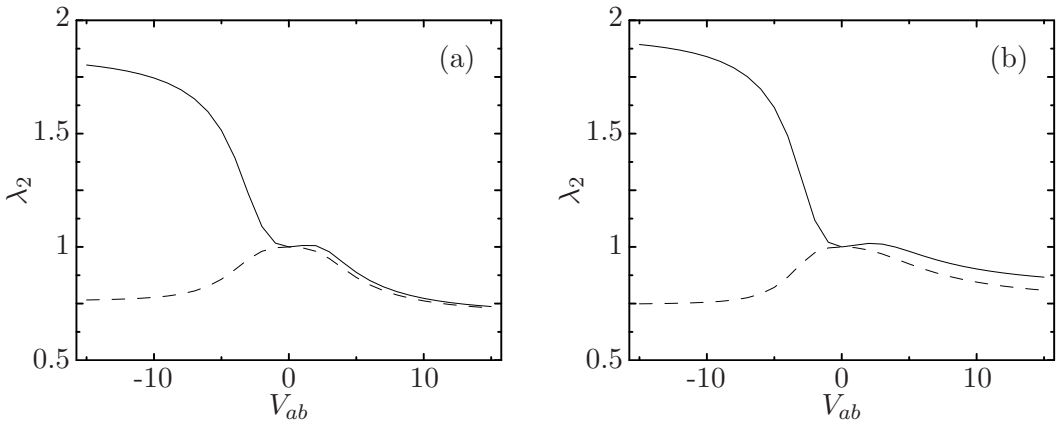

Figure 4.4: The solid line shows the dependence of the largest eigenvalue λ_2 of $\rho^{(2)}$ as a function of interaction strength. The dashed line shows the 2nd largest eigenvalue. (a), results for a 10-5-5-ff system ($I = 10$ lattice sites, $N_a = N_b = 5$ particles both species fermionic) and (b), results for a 12-5-5-ff system.

to single particles in bosonic systems at small interaction strength. For $V_{ab}/J = 0$ the pair coherence function is zero $S(\delta) = 0$ because the groundstate is a Slater determinant and the two-body density matrix equals the product of the one-body density matrices.

We already mentioned that in fermionic systems the one-body density matrix cannot exhibit ODLRO because the eigenvalues (occupation numbers) of the natural orbitals (Bloch functions) have to be smaller than or equal to one, $\lambda_1 = n_q \leq 1$. Obviously, the two-body density matrix shows ODLRO. Therefore there should be a macroscopic eigenvalue of $\rho^{(2)}$. This is depicted in figure 4.4. The finite value at the tail of the pair coherence function as well as the plot of λ_2 may be a hint that a pair of particles of species a and species b form the basic group in the regime of attractive interactions. The existence of an eigenvalue λ_2 that is of the order N is hard to verify strictly in our small-sized systems. But we see that λ_2 changes significantly when entering the regime of attractive interactions and separates clearly from the second largest eigenvalue.

4.3 Quasimomentum Correlation Function

Keeping in mind the spatial delocalisation of particle pairs, one would expect this feature to appear as a peak in momentum space. Actually the existence of a macroscopic eigenvalue λ_2 of the two-body density matrix $\rho^{(2)}$ observed in figure 4.4 is a hint that there is a favoured two-particle state. In order to obtain more insight, we define the quasimomentum correlation function $C_{ab}(q, q')$

$$\begin{aligned} C_{ab}(q,q') &\equiv \left\langle \psi \,\middle|\, \hat{n}_q^{(a)}\hat{n}_{q'}^{(b)} \,\middle|\, \psi \right\rangle - \left\langle \psi \,\middle|\, \hat{n}_q^{(a)} \,\middle|\, \psi \right\rangle \left\langle \psi \,\middle|\, \hat{n}_{q'}^{(b)} \,\middle|\, \psi \right\rangle , \qquad (4.5) \\ \text{with} \quad \hat{n}_q^{(a)} &\equiv \hat{c}_q^\dagger \hat{c}_q \otimes \hat{1} , \\ \text{and} \quad \hat{n}_q^{(b)} &\equiv \hat{1} \otimes \hat{c}_q^\dagger \hat{c}_q . \end{aligned}$$

This correlation function is composed of the unitarily transformed matrices $\tilde{\rho}^{(1)}_{qq'}$ and $\tilde{\rho}^{(2)}_{qq',QQ'}$ we introduced in section 2.7. The indices $'ab'$ indicate that the two-body density matrix is again a mixed one. q describes the quasimomenta of species a and q' of species b respectively. $\hat{n}_q^{(a,b)}$ are the quasimomentum occupation number operators acting on the respective species.

Figure 4.5 depicts all possible combinations for q and q' at a fixed attractive interaction strength. The large values at the diagonal show that the system exhibits a $(q,-q)$-correlation. If the quasimomentum q is occupied with a particle of species a, the system tends to occupy the quasimomentum $-q$ with a particle of species b. Thus, besides the pairing in coordinate space, there is a $(q,-q)$-pairing in momentum space as well. In a pictorial view the $(q,-q)$-pairing leads to a formation of standing waves. The resulting two-particle wavefunction is similar to ψ^+ (2.13) and thus minimises the energy. In BCS theory, the pairing of electrons in momentum space – known as Cooper-Pair formation – is responsible for superconductivity. There, attractive interactions between electrons are generated via the coupling to phonons. Other momenta are almost not correlated. For repulsive interactions this is quite different. Figure 4.6 shows that the 12-5-5-ff system exhibits practically no correlation in the regime of repulsive interactions, whereas the Mott-like 10-5-5-ff system shows anticorrelation for $|q-q'| = 5$. If a particle of species a occupies $q = 0$ it 'blocks' particles of species b to occupy $q = 5$, similarly $q = 1, -1$ block $q = -4, 4$, and so on. We will come back to this point later during the discussion of the insulating behaviour of half-filled systems.

In order to obtain a detailed view of how the momentum correlation changes as function of the interaction strength, we fix the values for the quasimomenta $q = -q'$ and plot

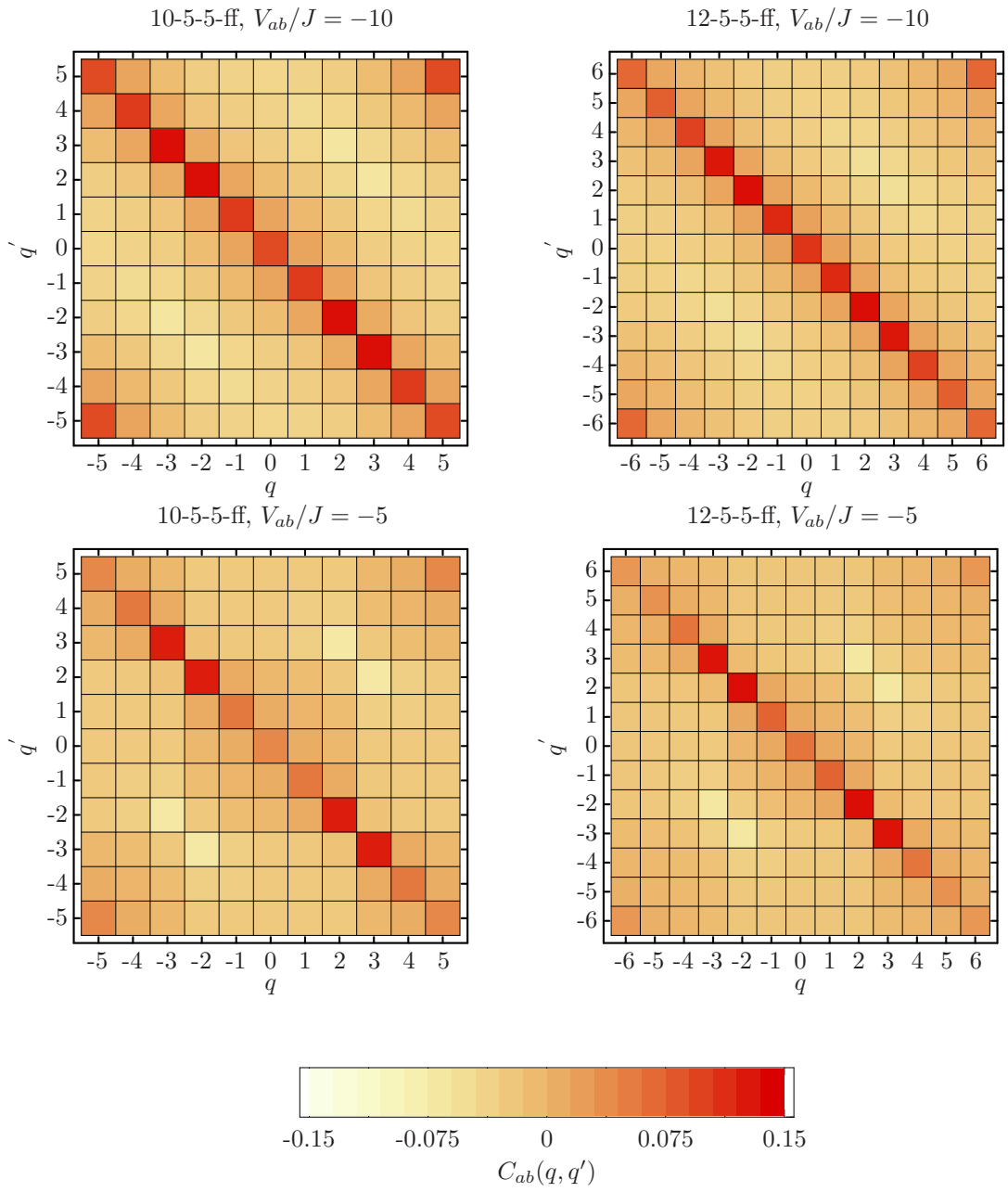

Figure 4.5: The quasi-momentum correlation function $C_{ab}(q, q')$ at fixed interaction strength for all combinations of q and q'. Top left: 10-5-5-ff system, top right 12-5-5-ff system, both at $V_{ab}/J = -10$. Bottom left: 10-5-5-ff system, bottom right 12-5-5-ff system, both at $V_{ab}/J = -5$. The bottom bar shows the colour coding.

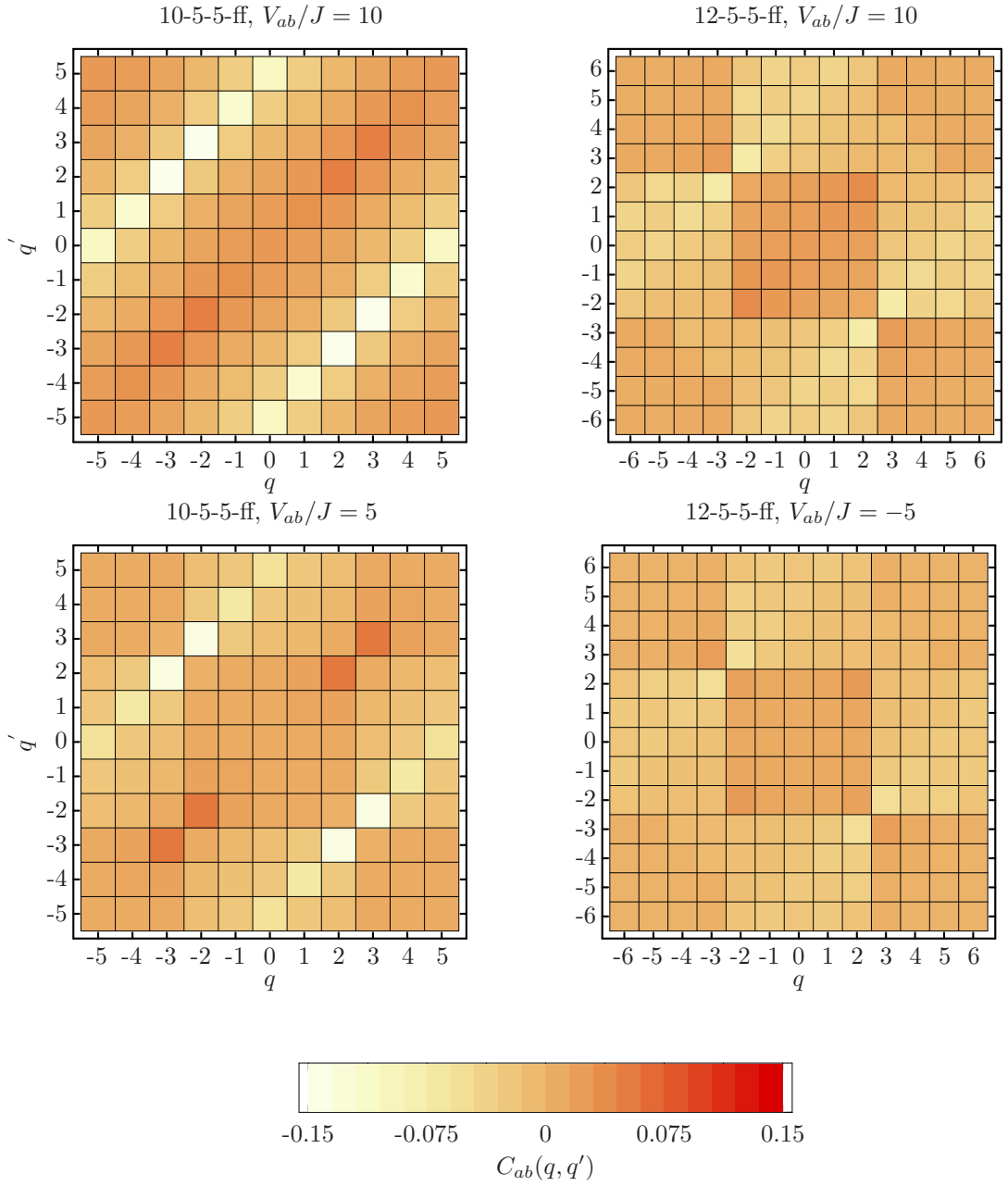

Figure 4.6: cf. figure 4.5. Top left: 10-5-5-ff system, top right: 12-5-5-ff system, both at $V_{ab}/J = 10$. Bottom left: 10-5-5-ff system, bottom right: 12-5-5-ff system, both at $V_{ab}/J = 5$. The bottom bar shows the colour coding.

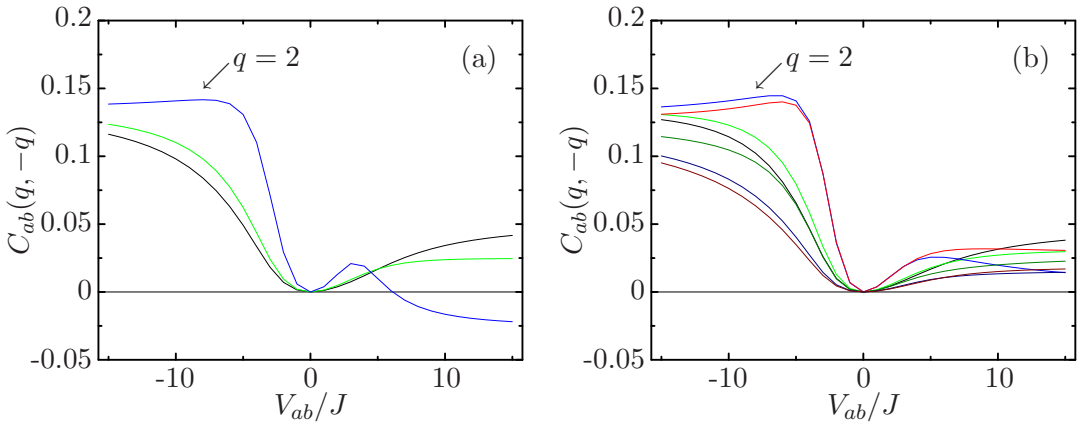

Figure 4.7: The quasi-momentum correlation function $C_{ab}(q,-q)$ for fixed quasimomenta $q=-q'$ as function of the interaction strength. (a) 10-5-5-ff system and (b) 12-5-5-ff system. The colour coding is: $q=0$ (black), $q=1$ (green), $q=2$ (blue), $q=3$ (red), $q=4$ (dark green), $q=5$ (dark blue), $q=6$ (dark red). In the 10-5-5-ff system some correlations are degenerate due to particle-hole symmetry.

the correlation function $C_{ab}(q,-q)$ as function of the interaction strength. Figure 4.7 reveals that for particles at the Fermi surface ($q=2$) the $(q,-q)$-correlation increases rapidly once it enters the regime of attractive interactions and reaches a maximum at $V_{ab}/J \approx -5$. For strongly attractive interactions, the $(q,-q)$-correlations become roughly equal for all momenta. In the 10-5-5-ff system there are only three lines visible because of the particle-hole symmetry (there are as many particles as holes). Thus, annihilating a particle with quasimomentum q is similar to creating a hole with $-q$. We could describe such a symmetric system in terms of holes instead of particles without any differences. In a non-interacting system, $q=2$ is the last occupied particle state and $q=3$ is the first occupied hole state. The symmetry remains also at non-zero interaction strengths, implying $C_{ab}(2,-2)=C_{ab}(3,-3)$ and $C_{ab}(1,-1)=C_{ab}(4,-4)$ for all interaction strength. In the 12-5-5-ff system, there are more holes than particles and, therefore, this symmetry is broken and all possible combinations appear.

4.4 Transport Properties – Drude Weight

A question that arises immediately when talking about fermions on a periodic lattice is whether the system is an insulator, a conductor or even a superconductor. First of all we define, what we are going to talking about. More detailed information can be found in [18].

In general, one distinguishes four different types of insulators [18]. The first one – and surely most common – is the Bloch-Wilson or band insulator. As mentioned in section 2.1, electrons in a lattice may be described by a set of Bloch functions spanning the energy bands. Those energy bands are separated by a so called energy gap (2.15). The size of the gap depends on the potential geometry, i.e., the interaction with the ion-cores that form the lattice. In a conductor one band is partly filled (conduction band) and it is possible – e.g. with an electric field – to shift the Fermi sphere away from equilibrium and provide a net momentum of the electrons occupying that band. The situation is illustrated in figure 4.8. In a band insulator, the upper band is completely filled (valence band) and thus the Fermi sphere cannot be shifted, because it would enter the next Brillouin zone. Note that the distances between the quasimomenta have to remain constant, i.e., an integer multiple of $2\pi/I$. Therefore, it is not possible to establish an (electric) current. If an energy band is completely filled but the energy gap is small such that thermal excitations are able to push electrons to the next higher band, one talks about a semi conductor. For completeness we mention two other, but similar types of insulators that depend on single-electron properties. The Peierls insulators are those that result from lattice deformations and Anderson insulators result from lattice impurities. The class of insulators we discuss are Mott insulators that are solely driven by two-body interactions. In the following we restrict ourselves to zero-temperature systems and investigate the conductivity, i.e., the response of the system to a moderate (electric) field. As a direct result of band theory we find that a system of two fermion species, each with half-filling and repulsive interactions strong enough to suppress tunnelling becomes an insulator. In a band insulator, the Pauli principle forbids two particles to occupy the same lattice site, whereas the same effect is obtained by the repulsive interaction here. Namely, in the regime of repulsive interactions the two species perform a mutual blocking of quasimomentum states. The unfilled dots in figure 4.8 which are free quasimomentum states then get blocked by particles of the other species and detains the Fermi sphere to be shifted.

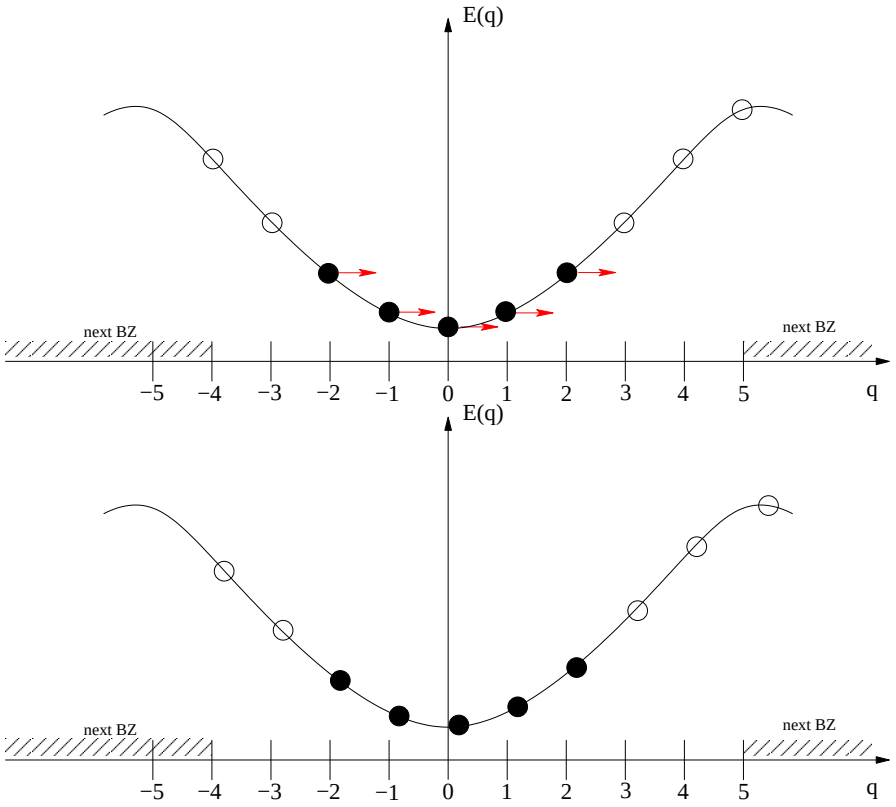

Figure 4.8: Shift of the Fermi sphere by an application of a phase twist (red arrows). The picture shows exemplary one species of a 10-5-5-ff system at interaction strength zero. The filled dots are particles and the open ones are free quasimomentum states (holes). The holes are allowed to enter the next Brillouin zone. Repulsive interactions lead to blocking of the quasimomentum states by the other species and prevent a shift of the Fermi sphere.

In connection with current and conductivity, one might first ask how the energy of the system changes when an external potential is applied. This energy might be considered as the kinetic energy of the moving particles. We can think again of the two-fluid picture discussed in section 3.4. Either there is a response to the external field and the groundstate energy increases or the system is not affected by the potential and the groundstate energy remains constant. Again, we use that a potential gradient can be expressed in terms of twisted boundary conditions with twist angle Θ. With the groundstate energy $E(\Theta = 0) = E_0$ and a sufficiently small twist angle Θ, we write down the Taylor expansion of the energy as function of Θ up to the second order

$$E(\Theta) \approx E_0 + \frac{\partial}{\partial\Theta} E(\Theta)\Big|_{\Theta=0} \cdot \Theta + \frac{1}{2} \frac{\partial^2}{\partial\Theta^2} E(\Theta)\Big|_{\Theta=0} \cdot \Theta^2 + O(\Theta^3) \,. \tag{4.6}$$

This is closely related to the standard way of deriving an expression for the real part of dc conductivity from linear response theory [18]. The first derivative vanishes at $\Theta = 0$ because the groundstate energy should be minimal. The second derivative is a quantity that is proportional to the 'movability' of the particles. For insulators this will be zero because their energies are not affected by the external potential, whereas the more the energy increases the more the particles respond to the potential. From equation (4.6) we can derive an approximation for the second derivative:

$$\frac{\partial^2}{\partial\Theta^2}\, E(\Theta)\,\Big|_{\Theta=0} \approx 2\frac{E(\Theta) - E_0}{\Theta^2}\ . \tag{4.7}$$

The right-hand term already appeared during the discussion of the superfluid fraction (3.18). Using the same prefactors we define the Drude weight [21]

$$f_d \equiv \frac{I^2}{JN}\frac{E_\Theta - E_0}{\Theta^2}\ . \tag{4.8}$$

First we investigate how the energy of the twisted state depends on Θ. The numerical results for the 10-5-5-ff system are shown in figure 4.9. At interaction strength zero the dispersion relation is again the one of a free particle and we observe a level crossing at $\Theta = \pi$. In the regime of repulsive interactions level repulsion occurs and leads to a deformation of the parabola. This is in agreement with the phenomenology observed for bosonic systems (figure 3.5). With increasing attractive interaction strengths, the level crossing is shifted to smaller values of Θ. The Drude weight should not depend on the value of Θ. Thus we use $\Theta = 0.1$ for all calculations of the Drude weight where the deviation from the parabola is negligible for all interaction strengths.

There are two possibilities to apply the twist. We can push the two species into the same direction or into opposite directions. This is called twist and countertwist, respectively. Before we try to understand the numerical results we should mention that particle-hole symmetry plays a significant role. Moving particles in one direction we may likewise think of moving holes of the same species in the other direction. In the same manner an attractive interaction between species a and b means a repulsive one between species a and holes of species b and vice versa. But one must not mix up the two pictures, either we consider holes or we consider particles within the species.

We first discuss the twist. As shown in figure 4.10 in the regime of attractive interactions the Drude weight decreases, but remains finite, for both systems with increasing interaction strengths V_{ab}/J. One might be tempted to regard the system as half filled and consisting of composite particles. In momentum space there should be enough room

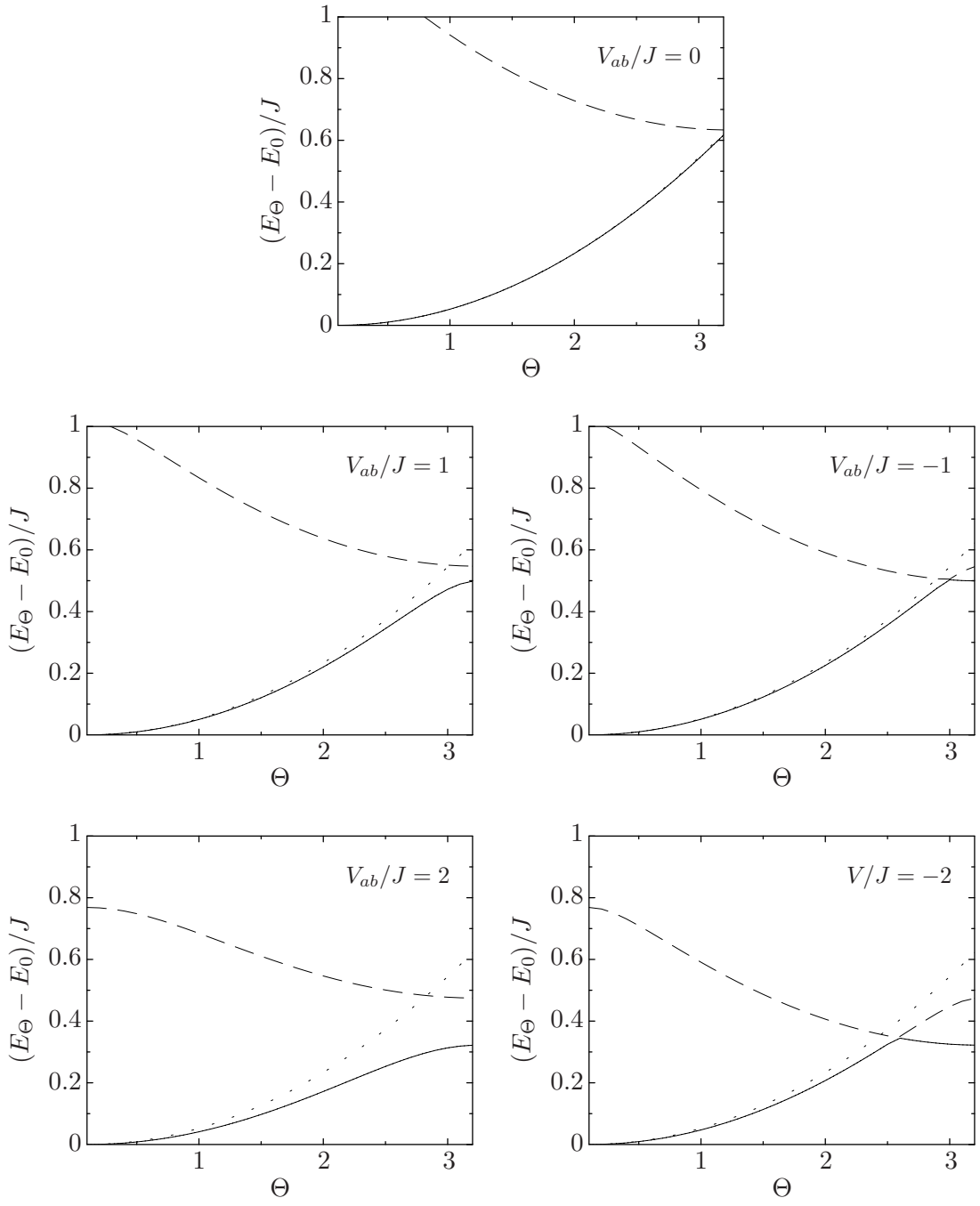

Figure 4.9: The solid lines show the difference of the groundstate energies of the twisted and the untwisted Hamiltonians for a 10-5-5-ff system. The dashed lines show the difference of the first excited state of the twisted and the groundstate of the untwisted Hamiltonian. The dotted line is the kinetic energy of a free particle $E(\Theta) \propto \Theta^2$. Top left to bottom right: $V_{ab}/J = 0$, $V_{ab}/J = 1$, $V_{ab}/J = -1$, $V_{ab}/J = 2$ and $V_{ab}/J = -2$.

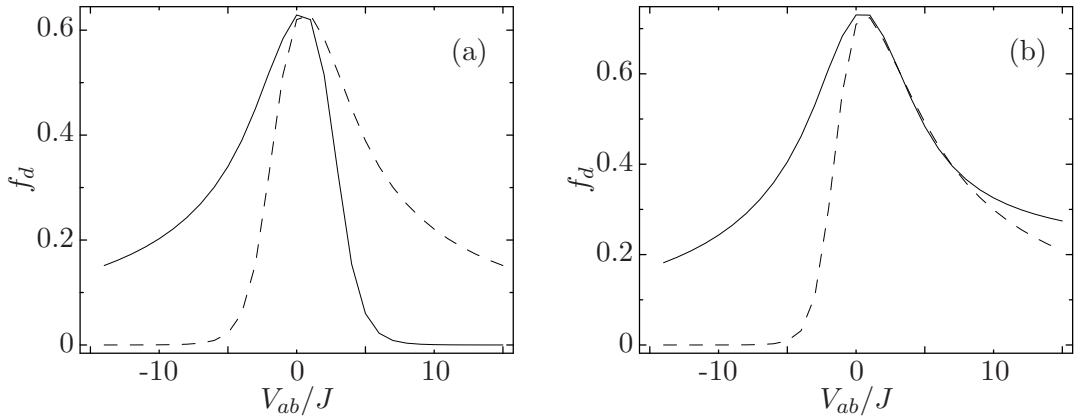

Figure 4.10: (a) Drude weight for the 10-5-5-ff system and (b) for the 12-5-5-ff system as function of the interaction strength. Solid line corresponds to the twist and dashed line to the countertwist.

to shift the Fermi sphere and establish a flow, but then the question arises why the Drude weight decreases. We can understand this with the help of the quasi-momentum correlation function (4.5). In the regime of attractive interaction strengths the system exhibits $(q, -q)$-pairing. Thus, if the external potential tries to shift a particle of species a to a quasimomentum q, the system wants to occupy the quasimomentum $(-q)$-state with a particle of species b. This prevents the system from establishing a net flow and thus suppresses the Drude weight. For repulsive interactions the half-filled 10-5-5-ff system and the non-half-filled 12-5-5-ff system differ. In the half-filled case the Drude weight decreases rapidly and vanishes completely at $V_{ab}/J \approx 5$. Although the species also perform a mutual blocking of momentum space in case of the non-half-filled system, there is room left in momentum space for a net flow even at large repulsive interaction strengths.

The countertwist reveals the perfect particle-hole symmetry for the half-filled system. One simply has to consider particles of species a and holes of species b moving in the same direction, change the sign of the interaction and ends up at the same result as for the twist. For the non-half-filled system this symmetry does not exist. Using the particle-particle picture we can understand the decline at $V_{ab}/J \approx -5$ for both systems. Because the interaction forces the particles to stick to each other, they cannot move into opposite directions and, therefore, the Drude weight for the countertwist vanishes.

We should mention that this behaviour of the Drude weight has been already calculated by Kawakami and Yang [23] in 1991 with a finite-size scaling method based upon a

Bethe-ansatz solution. The numerical values for the non-half-filled 12-5-5-ff system are in good agreement. However, due to their extrapolation to the thermodynamic limit, they predict a vanishing Drude weight for half-filled (like 10-5-5-ff) systems for any positive interaction $V_{ab}/J > 0$. Hence, once again we are reminded of the inherent finite-size effects of our approach.

We made an interesting observation for systems with even numbers of particles, e.g., a 10-4-4-ff system. In this case, the Drude weight at interaction strength zero becomes negative. First we thought of a failure of the Lanczos algorithm to compute degenerate eigenvalues. But looking at figure 4.11 of the shifted Fermi sphere one can understand what happens: the particles can indeed lower their energy when a flow is present. The minimum of the groundstate energy should be at a flow that equals half the value of the distance between the quasimomenta $\Delta q = 2\pi/I$. Figure 4.12 shows that the energy minimum of the system is exactly at a twist angle that equals π. From the twisted Hamiltonian (3.20), we see that applying this twist angle is indeed similar to adding $\frac{1}{2}\Delta q$.

$$q_{twist} = \Theta/I = \pi/I = q_{1/2} \tag{4.9}$$

The untwisted system is not capable of showing those shifted quasimomenta $\tilde{q}_l \equiv q_l + q_{twist}$ because they do not fulfil the periodic boundary conditions. Maybe this effect might be absorbed by neglecting the anticommutation relations during the process of basis construction, because they are responsible for the anti-periodic boundary conditions. However, a definitive statement will need further investigations.

Due to the small system sizes and the resulting finite size effects, our major task for the future will be to get rid of the size limitation using different numerical as well as conceptional approaches to tackle the problem of quantum gases on lattices.

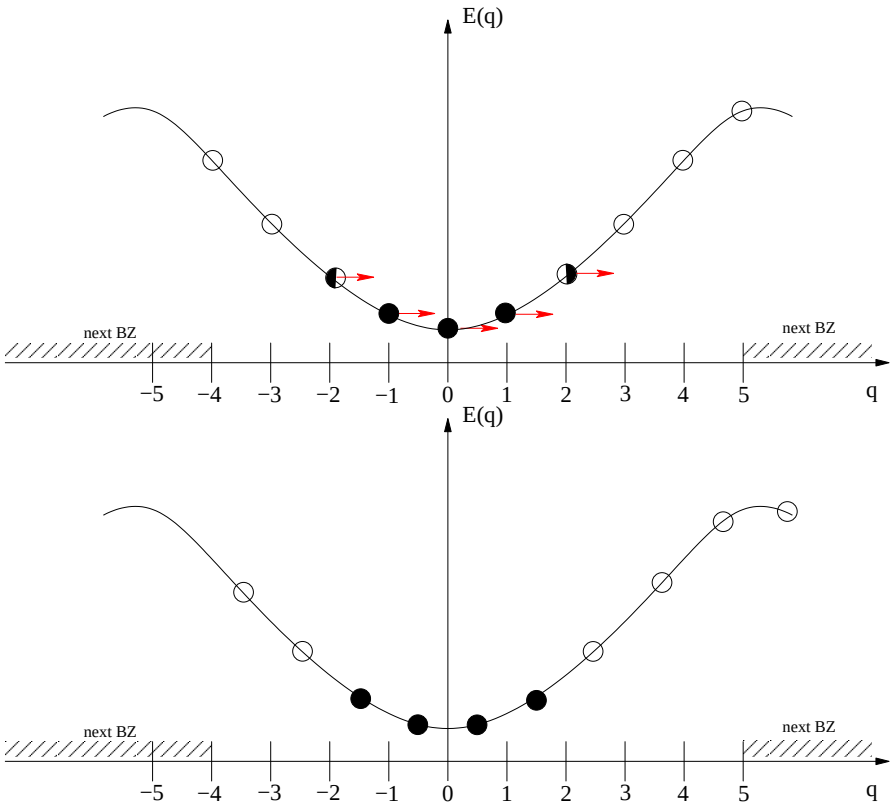

Figure 4.11: Shift of the Fermi sphere by an application of a phase twist (red arrows) for a 10-4-4-ff system.

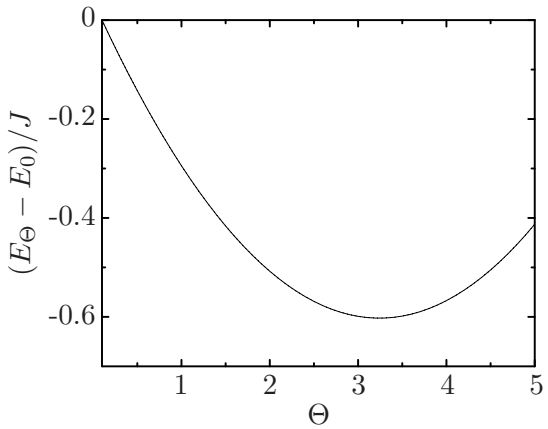

Figure 4.12: The plot shows the energy difference $(E_\Theta - E_0)$ as function of the twist angle for a 10-4-4-ff system with an even number of fermions. The energy minimum is at $\Theta = \pi$ which corresponds to $\frac{1}{2}\Delta q = \frac{\pi}{I}$.

Chapter 5

Outlook – Bose-Fermi-Mixtures

5.1 Bose-Fermi Hubbard Model

Bose-Fermi mixtures in optical lattices provide an interesting environment of mixed quantum statistics. We will investigate several special regimes in the rich phase-diagram of those mixtures. In the following, the references to equations have to be handled with care since they were defined for boson and fermion-fermion systems. Consider them as an 'analogous to' reference.

Similar to the Fermi-Fermi Hubbard Hamiltonian, we introduce the Bose-Fermi Hubbard Hamiltonian. Now, the operators $\hat{a}_l^\dagger, \hat{a}_l$ and $\hat{n}_l^{(a)}$ act on the bosonic species and the operators $\hat{b}_l^\dagger, \hat{b}_l$ and $\hat{n}_l^{(b)}$ on the fermionic species. Again, there is an on-site interaction between the species V_{ab} but also an on-site interaction within the bosonic species V_{aa}. Hence, the Bose-Fermi-Hubbard Hamiltonian reads [21]:

$$\hat{H} = -J\sum_{l=1}^{I}\Big(\hat{a}_{l+1}^\dagger\hat{a}_l + \hat{b}_{l+1}^\dagger\hat{b}_l + h.a.\Big) + V_{ab}\sum_{l=1}^{I}\hat{n}_l^{(a)}\,\hat{n}_l^{(b)} + \frac{1}{2}V_{aa}\sum_{l=1}^{I}\hat{n}_l^{(a)}(\hat{n}_l^{(a)}-1)\,. \tag{5.1}$$

Due to the second interaction term, there are two parameters V_{ab}/J and V_{aa}/J now. The groundstate is a sum over tensor products of all possible combinations of the two species' Fock states where the first Ket denotes the bosonic species and the second Ket the fermionic component

$$\mid \psi \rangle \equiv \sum_{\alpha=1}^{D_a}\sum_{\beta=1}^{D_b} C_{\alpha\beta} \mid \{n_1^{(a)},\dots,n_I^{(a)}\}_\alpha \rangle \otimes \mid \{n_1^{(b)},\dots,n_I^{(b)}\}_\beta \rangle\,. \tag{5.2}$$

The coefficients $C_{\alpha\beta}$ are obtained by solving the eigenproblem of the Hamilton matrix analogue to (2.45).

In the following, we will examine a system with $I = 10$ lattice sites and $N_a = N_b = 5$ bosonic and fermionic particles. The dimension of the basis is $D_a \cdot D_b = 504504$.

5.2 Simple Observables

Given that there is no external trapping potential and we use periodic boundary conditions, the mean occupation number $n_l^{(a)}$ (3.1) is again constant and equals the filling rate of the respective species. As a result of the idempotent fermionic occupation number operator, the fluctuation of the fermionic species is also constant for all interaction strengths (4.3). The first non-trivial observables is the fluctuation of the bosonic species (3.2)

$$\sigma^2 \equiv \sigma_l^2 \left\langle \psi \right| (\hat{n}_l^{(a)})^2 \left| \psi \right\rangle - \left\langle \psi \right| \hat{n}_l^{(a)} \left| \psi \right\rangle^2 \tag{5.3}$$

and the maximum coefficient of the groundstate C_{max}^2 (3.3)

$$C_{max}^2 \equiv \max(C_{\alpha\beta}^2) \; . \tag{5.4}$$

The numerical results for these quantities are depicted in figure 5.1. The maximum coefficient reveals that there are several different regions within the V_{aa}-V_{ab}-plane. Note that the plot shows $C_{max}^2 \cdot 20$ in order to be richer in contrast. Within two rectangular areas both parallel to the axes the groundstates are composed of a superposition of many Fock states. From the fluctuations of the bosonic particles along the V_{ab} axis one can assume that those with strongly fluctuating bosonic occupation numbers are among them. The two regions (A) and (B) exhibit a structure of the respective groundstates where only a few Fock states dominate. We will see in section 5.4 what particular kinds of Fock states contribute. Finally, there is a transition region at $V_{ab} \approx 2V_{aa}$ that is again made up of many Fock states, but with suppressed bosonic fluctuations.

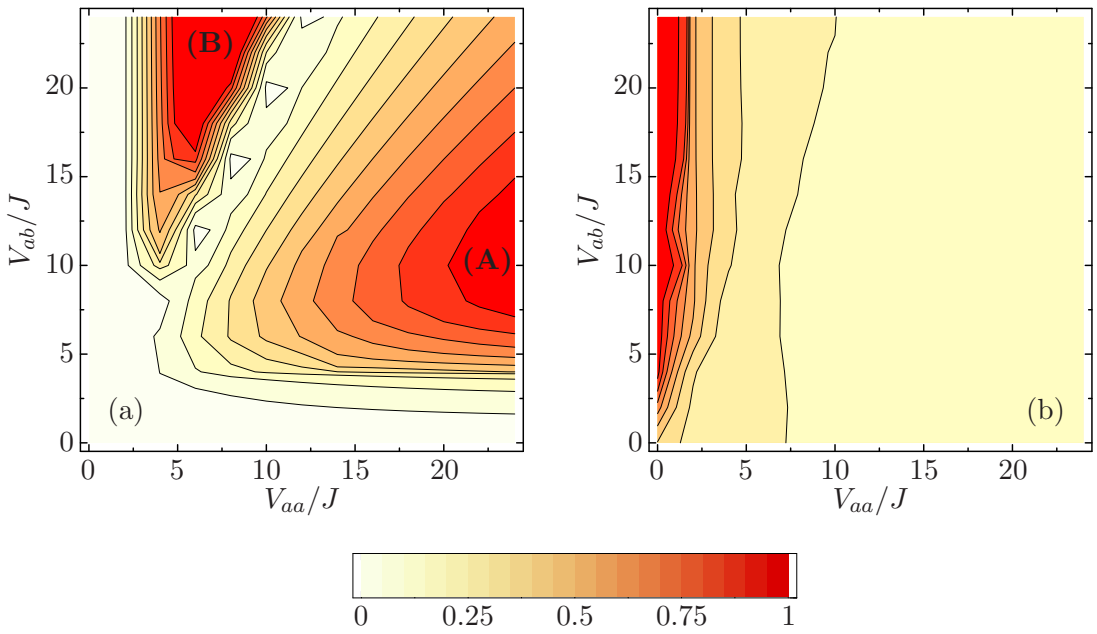

Figure 5.1: Panel (a) shows the the maximum coefficient $C^2_{max} \cdot 20$ and reveals two regions (A) and (B) where only a few Fock states dominate. Panel (b) shows the fluctuation σ^2 of the bosonic species. Both for a 10-5-5-bf system.

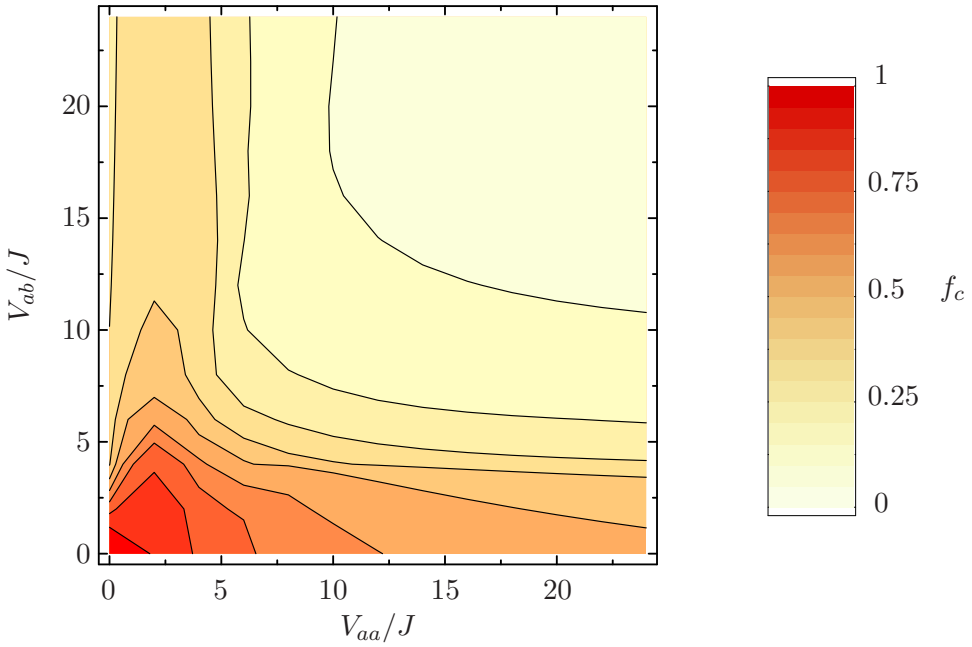

Figure 5.2: Condensate fraction f_c of the bosonic species in a 10-5-5-bf system as function of V_{aa}/J and V_{ab}/J.

5.3 Condensate Fraction

The bosonic particles that occupy the lowest single-particle state form a Bose-Einstein condensate. According to section 3.2 we define the condensate fraction f_c as the largest eigenvalue λ_1 of the one-body density matrix $\rho^{(1)}$ divided by the total number of bosonic particles N_a.

$$f_c \equiv N_c/N_a = \lambda_1/N_a. \tag{5.5}$$

The numerical results are shown in figure 5.2. Although the fluctuation of the bosonic species in the regime of small boson-boson and large boson-fermion interaction strengths is large, the condensate fraction depletes rapidely. This might be a hint that there is a preferred Fock state structure within the bosonic species, that does not fit for the quasimomentum zero state. As expected, the depletion of the condensate for increasing boson-boson interactions is rather slow due to the small filling factor (cf. figure 3.2). In the following section we will see that there are indeed different preferred structures depending on the position in the interaction scheme.

5.4 Density-Density Correlation

For a more detailed investigation of the different phases and the underlying structure we define the density-density correlation function $D(\delta)$. We use those matrix elements that annihilate and create a fermion at lattice site $1+\delta$ and annihilate and create a boson at site 1:

$$\begin{aligned} D(\delta) &\equiv \langle \psi \mid \hat{a}_1^\dagger \hat{b}_{1+\delta}^\dagger \hat{b}_{1+\delta} \hat{a}_1 \mid \psi \rangle \\ &\quad - \langle \psi \mid \hat{a}_1^\dagger \hat{a}_1 \mid \psi \rangle \langle \psi \mid \hat{b}_{1+\delta}^\dagger \hat{b}_{1+\delta} \mid \psi \rangle \\ &= \langle \psi \mid \hat{n}_1^{(a)} \hat{n}_{1+\delta}^{(b)} \mid \psi \rangle - \underbrace{\langle \psi \mid \hat{n}_1^{(a)} \mid \psi \rangle \langle \psi \mid \hat{n}_{1+\delta}^{(b)} \mid \psi \rangle}_{const} . \end{aligned} \tag{5.6}$$

Due to the constant mean occupation numbers at each site, which equal the filling rate of the lattice, the product of the one-body density matrix elements is constant, too. The numerical results depicted in figure 5.3 show that the behaviour of the particles in the two regimes is completely different. In the region of large boson-fermion and small boson-boson interaction strengths (B) the system exhibits a block separation. As soon as as the distance δ becomes larger than two lattice sites, the density-coherence function changes its sign. The boson occupying lattice site 1 is sourrounded by the 4 remaining bosons but at $\delta \geq 3$ there must be the first fermion. We can understand this by considering a single hopping process. Hopping of a boson to a lattice site that is occupied by a fermion is energetically more expensive than hopping to a lattice site that is occupied by a boson. Thus bosons cluster in order to enable tunnelling with less effort. In region (A) where the boson-boson interaction dominates, the system shows an alternating occupation of lattice sites with bosons and fermions. Here tunnelling to a lattice site that is occupied by the other species is energetically favoured and causes the alternating occupation. We also probe for density correlations in an interaction regime similar to the attractive fermion-fermion systems with large boson-boson repulsion – as an equivalent to the Pauli principle – and an attractive interaction between bosons and fermions. Besides the on-site correlation caused by the attractive boson-fermion interaction, there is no significant correlation for larger distances.

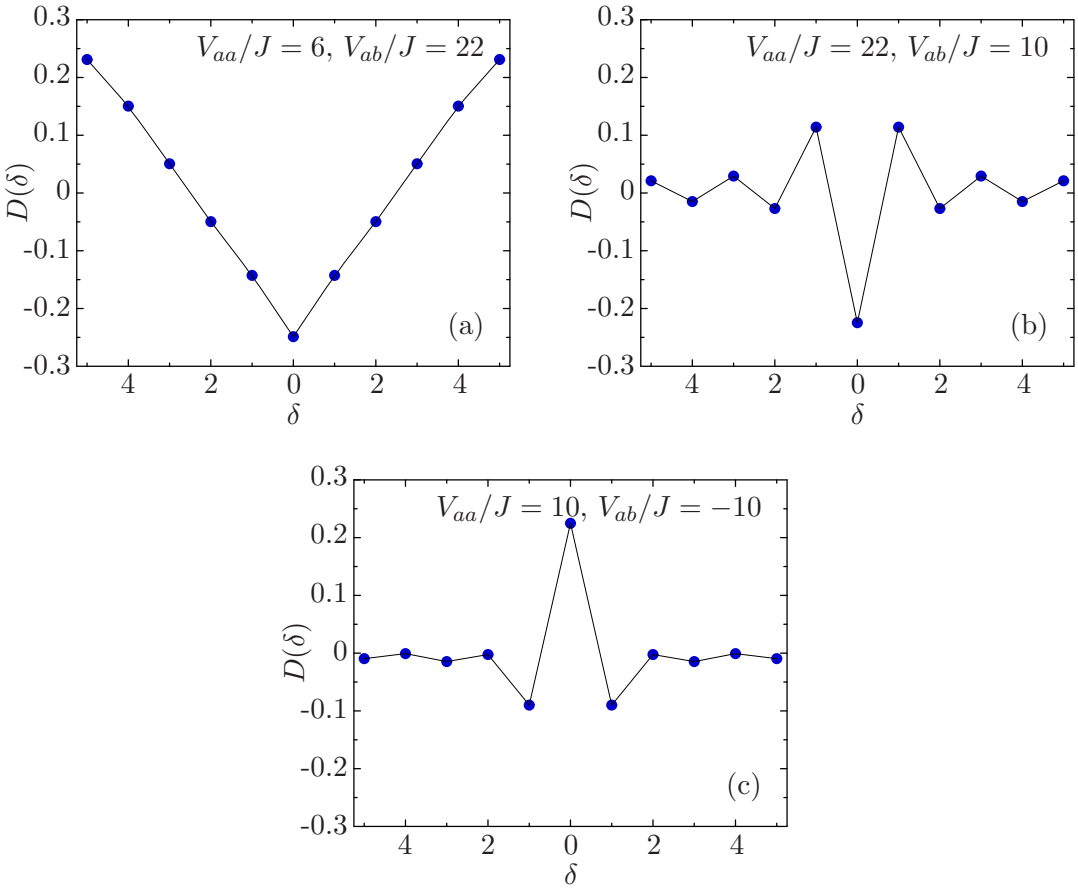

Figure 5.3: The density correlations in the two different phases are plotted as function of the lattice distance δ. (a) the system exhibits a block separation in region (B) ($V_{aa}/J = 6$, $V_{ab}/J = 22$). (b) at region (A) ($V_{aa}/J = 22$, $V_{ab}/J = 10$) there is an alternating occupation of lattice sites. (c) an environment similar to attractive fermion-fermion systems ($V_{aa}/J = 10$, $V_{ab}/J = -10$), but without significant correlations.

5.5 Pair Correlation

Similar to the pair coherence function we defined in section 4.2 for a fermion-fermion mixture, we can define a pair correlation function for the boson-fermion mixtures

$$\begin{aligned} \tilde{S}(\delta) \equiv & \left\langle \psi \right| \hat{a}_1^\dagger \hat{b}_1^\dagger \hat{b}_{1+\delta} \hat{a}_{1+\delta} \left| \psi \right\rangle \\ & - \left\langle \psi \right| \hat{a}_1^\dagger \hat{a}_{1+\delta} \left| \psi \right\rangle \left\langle \psi \right| \hat{b}_1^\dagger \hat{b}_{1+\delta} \left| \psi \right\rangle . \end{aligned} \tag{5.7}$$

This means we annihilate a boson-fermion pair at lattice site $1+\delta$ and create one at site 1. The numerical results shown in figure 5.4 reveal that besides the anticorrelation at the same lattice site due to the repulsive interaction, the pairs are almost uncorrelated, even in a situation similar to an attractive fermion-fermion system – with repulsive boson-boson and attractive boson-fermion interaction, there is no long-range pair-coherence present as observed in the fermion-fermion system (figure 4.3). The mixed statistics cause an alternating correlation anticorrelation pattern.

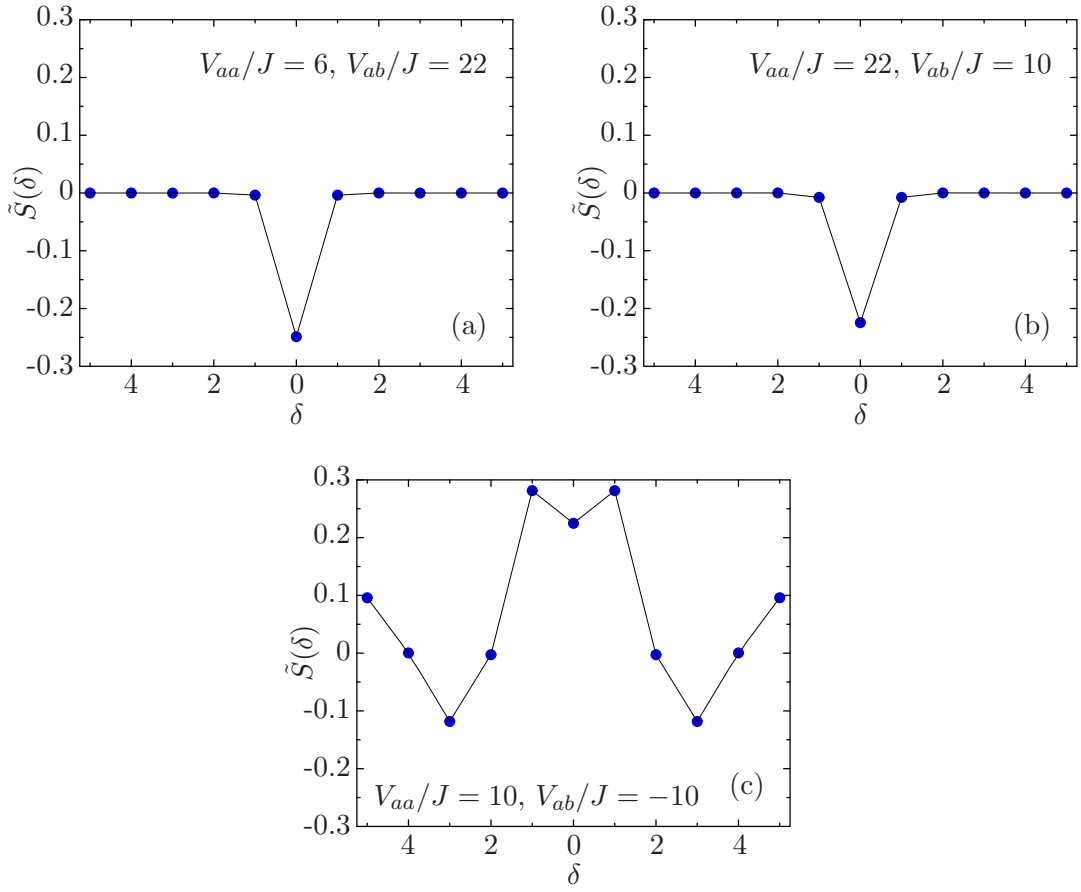

Figure 5.4: Pair correlation $\tilde{S}(\delta)$ as function of the distance δ. (a) region (B), ($V_{aa}/J = 6$, $V_{ab}/J = 22$). (b) region (A), ($V_{aa}/J = 22$, $V_{ab}/J = 10$). Besides the on-site anticorrelation due to the repulsive interaction, no correlation is present. (c) shows an environment similar to the attractive fermion-fermion systems ($V_{ab}/J = -10$, $V_{aa}/J = 10$). The mixed statistics system shows no long-range pair-coherence.

5.6 Quasimomentum Correlation Function

We define the quasi-momentum correlation function $\tilde{C}_{ab}(q,q')$ (4.5) to get an impression how the mixed statistics change the correlations in momentum space

$$\tilde{C}_{ab}(q,q') \equiv \left\langle \psi \right| \hat{n}_q^{(a)} \hat{n}_{q'}^{(b)} \left| \psi \right\rangle - \left\langle \psi \right| \hat{n}_q^{(a)} \left| \psi \right\rangle \left\langle \psi \right| \hat{n}_{q'}^{(b)} \left| \psi \right\rangle . \tag{5.8}$$

Again, the operators $\hat{n}_q^{(a)}$ act on the bosonic species and the $\hat{n}_{q'}^{(b)}$ on the fermionic species. The numerical results for the two regions (A) and (B) are depicted in figure 5.5. In region (B) the strong correlation at $q = q' = 0$ indicates that the quasimomentum zero Bloch function fits the block separation best. But notice that there is a small quasimomentum zero contribution in the bosonic part of the wavefunction (see figure 5.2). The 'S' structure in region (A) is indeed interesting, but its physical interpretation is not clear yet. In the environment similar to the attractive fermion-fermion system, there is a correlation between particular quasimomenta. But unlike the fermion-fermion systems where we observed large $(q,-q)$-correlations along the diagonal (figure 4.5), the (q,q') correlation pattern is not that intuitive in the case of mixed statistics.

In conclusion, we observed a much more difficult interplay in the boson-fermion system than in the fermion-fermion systems. We will have to put more effort into the investigation of boson-fermion mixtures in order to obtain a better understanding about the physics of systems with mixed quantum statistics.

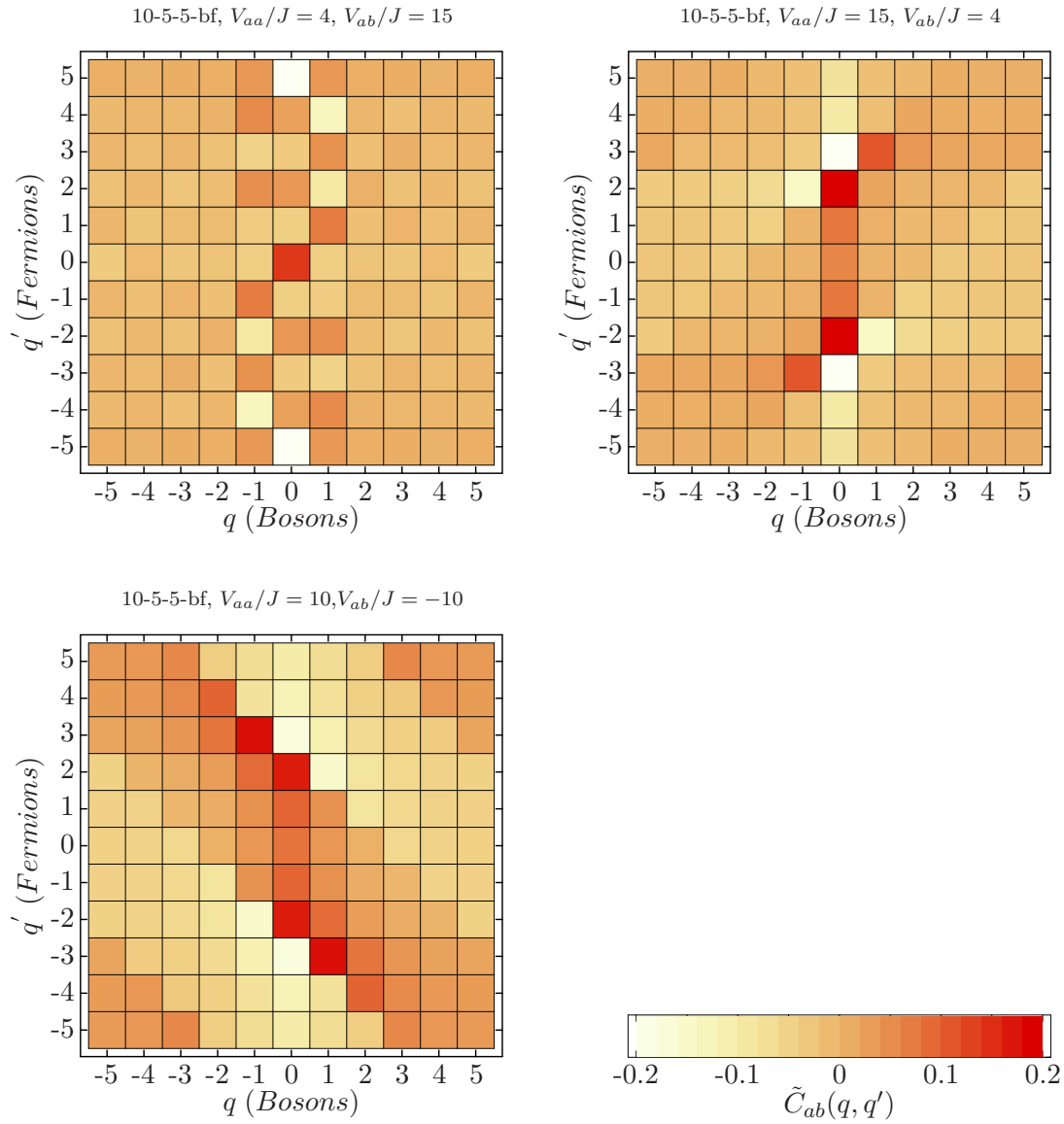

Figure 5.5: Quasimomentum correlations in the two different phases. Upper left panel: region (B) at $V_{aa}/J = 4$, $V_{ab}/J = 15$ and upper right panel: region (A) at $V_{aa} = 15$, $V_{ab} = 4$. The bottom left panel shows an environment similar to the attractive fermion-fermion systems, $V_{ab}/J = -10$, $V_{aa}/J = 10$.

Appendix A

Numerical Implementation & C++ Programs

A.1 Hamilton Matrix

All of our calculations are based upon the ground state $\mid \psi \rangle$ obtained by a diagonalisation of the Hamilton matrix. Since we are dealing with high-dimensional systems, it is required, on account of manageable CPU-time, to use sparse matrix algorithms like the Lanczos-based Arpack-Arnoldi algorithms [33]. Those depend crucially on the shape of the matrix to be diagonalised. It is desirable to have a band matrix with elements as close as possible to the diagonal. During our Mini-Research Markus Hild and I developed a basis creation algorithm that satisfies this demand.

Let us consider an $I = 6$, $N = 6$ bosonic system, for instance. We start with a Fock state that has all bosons at the first lattice site. By successively adding the hopping operators we compute related Fock states and the corresponding Hamilton matrix elements.

1 $\mid 6,0,0,0,0,0 \rangle$ startvector (first basis vector)

2 calculate $\hat{a}_2^\dagger \hat{a}_1 \mid 6,0,0,0,0,0 \rangle$

   (a) new $\mid 5,1,0,0,0,0 \rangle$ add new (first) matrix element $H_{2,1} = H_{1,2} = -J\sqrt{1 \cdot 6}$

   (b) search previously computed basis vectors to determine whether the new vector is already a basis vector
   yes: discard, no: add the vector to the basis

3 repeat the steps of 2 for all possible hopping operators

4 start over at step 1 for next (second) basis vector

The advantage of this algorithm is, that vectors are created directly from each other and, therefore, the elements of the hopping matrix are not far away from one another. One

avoids sorting the basis in a way where two related vectors are far away and produce a far off-diagonal matrix element. Unfortunately, the basis generation itself consumes a lot of CPU time, but it needs to be done only once.

The program that creates the basis and the hopping matrix is called 'hop'. Running 'hop' without any arguments yields the following usage information:

```
Usage: hop -II [Lattice-Sites] -SP [Number of species] -NN [n1 n2 .. nSP]
           -TYPES [ffbb...] -J [Tunnelling Strength] -o [outfile]
           -box (leave blank->cyclic)
```

As the prefix of the outfile we use the short form of the systems' description, e.g., 10-5-5-ff for a system with 10 lattice sites, 2 species of 5 fermionic particles each. A corresponding Bose-Fermi system is called 10-5-5-bf. The program has a simple process display and returns 2 files with the suffix '_bas.dat' and '_hop.dat' that contain the basis and the hopping matrix. The basis is stored in standard Mathematica rule format. The top of the 10-5-5-ff basis file reads

```
BASIS->{ {{1, 1, 1, 1, 1, 0, 0, 0, 0, 0},{1, 1, 1, 1, 1, 0, 0, 0, 0, 0}},
         {{1, 1, 1, 1, 0, 1, 0, 0, 0, 0},{1, 1, 1, 1, 1, 0, 0, 0, 0, 0}},
                                         .
                                         .
                                         .
       }
```

The hopping matrix is stored in a sparse matrix format where each line has three values: the first and the second denote the position in the matrix (n, m) and the third is the corresponding floating point value. Using this matrix format it is possible to compute a matrix vector product in a single loop through the lines of the matrix-file. m marks the vector component to be multipied with and n the component of the resulting vector the product must be added to. If one uses the '-box' switch, the basis has another sequence and the hopping matrix naturally has less values. In this case the filenames get the prefix '_noncyclic_hop/bas.dat'. There is another program 'hop_twisted' which generates a phase-twisted hopping matrix needed for the calculation of the Drude weight. Without arguments it prints:

```
Usage: hop_twisted -II [Lattice-Sites]
                   -SP [Number of species]
                   -NN [n1 n2 .. nSP]
                   -TYPES [ffbb...]
                   -J [Tunnelling Strength] default is 1
                   -o [outfile]
                   -TWIST [1|2|3|4] (1: sinusoidal twist-angle,
```

```
                                    2: constant twist-angle,
                                    3: gradient twist-angle,
                                    4: constant counter-twist-angle)
```

The switches for the twist that were used are 2 and 4. The basis file is similar to the cyclic non-twisted case but the third entry of the hopping matrix is a complex number of the form 'floating point + floating point * I'. The twist angle Θ is fixed to 0.1. For the calculations of the energy as function of the twist angle there is an independent program *transform_hop*.

A.2 Eigensystem Solver

After the creation of the basis and the hopping matrix, one has to add the interaction contributions and diagonalise the resulting matrix to obtain the groundstate. There are two programs, one for real Hamilton matrices (non-twisted) *chdiagREAL* and one for complex (twisted) ones *chdiagCOMPLEX*. Basically they are similar except that each of them use the respective Arpack Arnoldi routine – for real symmetric or for complex hermitian matrices – to solve the eigenproblem. It is sufficient to introduce one of them. Calling *chdiagREAL* without arguments prints to the screen:

```
Usage: chdiagREAL -c <config-file>
                  -vbf <from:to:step>
                  -vbb <from:to:step>
                  -debug <0|...|5>
                  -o <outfile-prefix> (default is '../results/arpack/result')
                  -which <LA|SA|SM|LM...> (default is SA)
                  -ose <onsite energy> (default is 0)
                  -e <num evals> (default is 5)
                  -evec <num vecs> (default is 1)
```

The config file contains information of the matrix to be diagonalised and looks like:

```
basis = ../BASES/10-5-5-ff_bas.dat
matrix = ../BASES/10-5-5-ff_hop.dat
species = 2
lattice = 10
dimension = 63504
types = ff
```

for a non-twisted 10-5-5-ff system. The 'vbf' option specifies the range of the interaction energy V_{ab} to be calculated. 'vbb' is the interspecies interaction for bosonic systems V_{aa}. One can tell the algorithm to compute the LargestAlgebraic, the SmallestAlgebraic, the

SmallstMagnitude and the LargestMagnitude eigenvalues and the corresponding eigenvectors. As we are always interested in the smallest algebraic ones, this is the default setting. The on-site energy option was used to check against our Mathematica results because its algorithm for solving eigenproblems is not able to compute the smallest algebraic values but only those that are smallest in magnitude. With a sufficiently large shift of the diagonal of the Hamilton matrix we could assure that the eigenvalue smallest in magnitude equals the smallest algebraic one. The last two switches tell the routine how many eigenvectors and eigenvalues are to be computed. The latest versions are also able to generate compressed output files in order to save disk space. An output file usually called coefficient file looks like this (exemplarily a 10-5-5-bf system):

```
{
   II->{10},
   SP->{2},
   NN-> {5, 5},
   FER-> {0,1},
   VBF-> {0.00},
   VBB-> {0.00},
   OSE-> {0.00},
   DD-> {504504},
   which-> {SA},
   EE-> { -16.4721359549996, -16.0901699437496, -16.0901699437495, ...},
   CC-> { -0.0000118033989, -0.0000263932023, -0.0000263932023, ...
                                        .
                                        .
                                        .
        }
}
```

The array EE contains the eigenvalues and CC the coefficients of the Fock states.

A.3 Density Matrices

The programs for computing the density matrices make use of the features of *C++* to define classes. There is a header file 'basis.h' in which the classes are defined. The private members of the class 'cFock' are an array with the length of the lattice to store the occupation numbers of each site, a boolean to distinguish between bosons and fermions, an integer, needed for the calculations of the anticommutation relations, and overloads for '=' and '=='. There are several prototypes of methods which implement creation and annihilation operators. The class 'cBasisVector' connects several (# of species) cFock

classes to a basis vector (2.44) and (4.2). Its private members are the number of species, the number of lattice sites, an array of cFock classes, an integer for its position in the coefficient file and an unsigned long long for a hash value. We will explain the hash value later on. Again, there are prototypes of methods to create and annihilate particles and so on. Finally, the class 'cBasis' is an array of cBasisVector and provides a method to read the basis file. The explicit methods are defined in 'basis.cpp' file. The files basis.h and basis.cpp are used in different programs and provide a mapping of the quantum mechanical operator formalism to C++.

Using these definitions, the program *c2bdm* becomes rather simple. It consists of a loop over the dimension of the basis with creation and annihilation operators acting on the groundstate. The problem is, that each time the operators act, and change the Fock state, one has to search the whole basis to find that new Fock state and multiply the coefficients. Again: For each matrix element, one has to do a loop over the dimension and in each step of the loop, one has to search the whole basis for the newly created Fock state. Note that in a system with $I = 10$ lattice sites one has to calculate $I^4 = 10000$ matrix elements for the two-body density matrix. In our first implementation we simply searched the basis in two directions from the actual unchanged Fock state. In the worst case scenario the calculation time of a single matrix element increases with $t \propto D^2$. Already in the 12-5-5-ff system with $D = 627264$ this was no longer feasible. Thus, we had to improve the search algorithm. The idea is, to provide each Fock state with a unique hash value and to sort the basis with respect to increasing hash values. For the hash values we use a number system with the base 'maximum number of particles per site (n_{max}) +1'. For a fermionic system this is the binary number system, for example. With the number of species S, the number of lattice sites I and the occupation number of the i-th site and the s-th species $n_{i,s}$, the hash value h of a Fock state reads:

$$h = \sum_{s=1}^{S} \sum_{i=1}^{I} n_{i,s} \cdot (n_{max} + 1)^{(i+s \cdot I)} \tag{A.1}$$

After calculating a Fock state and its hash value, we are immediately able to decide wether to jump up or down. The jump target is the middle of the remaining Fock states. The time required for the search is thus reduced to $t \propto ln(D)/ln(2)$.

The output file is similar to the coefficient file, but instead of the coefficients, the values of the matrix elements are stored. Calling *c2bdm* without arguments prints to the screen:

```
Usage: c2bdm -c [config-file] -b [1|2|mix] -part [dd|cor|full] -v [<from:to:step>]
```

```
-m [list-name]

-b:    Which Block of the Matrix should be computed ?
       1   = upper left
       2   = lower right
       mix = 1st & 3rd Quadrant (default is mix)

-part: dd   = density-density part
       cor  = correlation part
       full = full matrix (default is full)

-m:    Output in Mathematica-Rule-Format (list->{...}) optional
       list-name (default: twobody)
```

A.4 Transformation of the Hopping Matrix (Varying Θ)

The *transform_hop* program is used to calculate hopping matrices with varying twist angles Θ (e.g. figure 3.5 or figure 4.12). Calling without arguments *transform_hop* prints to the screen:

```
Usage: transform_hop -M [filename of hopping matrix]
                     -T twist angle [from:to:step] -N sites
```

For the diagonalisation, there is a modified program called *chdiag_transform* that simply has an additional switch which specifies the twist angle Θ to be computed.

A.5 Simple Observables

Observables that are directly accessible from the groundstate, like the mean occupation number, fluctuations and the maximum coefficient are calculated with *cobs*. Calling without arguments prints:

```
Usage: cobs -c [config-file]  -vbb -vbf [<from:to:step>]
```

The results are also stored using Mathematica rule format.

The various C++ programs were accompanied by some helpful Perl scripts (e.g., to

manipulate the data files or to start multiple calculations) and a handful of Mathematica notebooks which we consider not being worth to be explained in detail.

Bibliography

[1] M. H. Anderson, J. R. Ensher, M. R. Matthews, C. E. Wieman, and E. A. Cornell *Science* **269**, *198-201 (1995)*

[2] K.B. Davis, M.-O. Mewes, M.R. Andrews, N.J. van Druten, D.S. Durfee, D.M. Kurn, and W. Ketterle *Phys. Rev. Lett.* **75**, *3969-3973 (1995)*

[3] A. E. Leanhardt, T. A. Pasquini, M. Saba, A. Schirotzek, Y. Shin, D. Kielpinski, D. E. Pritchard, and W. Ketterle
Science **301**, *1513-1515 (2003)*

[4] K. W. Madison, F. Chevy, W. Wohlleben, J. Dalibard
cond-mat/0004037

[5] M. Greiner, C. A. Regal, and D. S Jin
Nature (London) **426**, *537-540 (2003)*

[6] D. Jaksch, C. Bruder, J. I. Cirac, C. W. Gardiner, and P. Zoller
Phys. Rev. Lett. **81**, *3108 (1998)*

[7] M.Greiner, O. Mandel, T. Esslinger, T.W. Hänsch and I. Bloch
Nature (London) **415**, *39 (2002)*

[8] T. Stöferle, H. Moritz, C. Schori, M. Köhl, and T. Esslinger
Phys. Rev. Lett. **92**, *130403 (2004)*

[9] H. Moritz, T. Stöferle, M. Köhl, and T. Esslinger
Phys. Rev. Lett. **91**, *250402 (2003)*

[10] F. Dalfovo, S. Giorgini, P. Pitaevskii and S. Stringari
Rev. Mod. Phys. **71**, *3 (1999)*

[11] J.E. Lye, L. Fallani, M. Modugno, D. Wiersma, C. Fort, M. Inguscio
cond-mat/0412167 (2004)

[12] Ch. Kittel
Einführung in die Festkörperphysik
Oldenbourg Verlag, 13. Auflage (1999)

[13] W. Jones and N.H. March, University of Rochester New York
Theoretical Solid State Physics Vol 1+2 (1973)

[14] T. Fliessbach, BI Wissenschaftsverlag
Statistische Physik (1992)

[15] J.J. Sakurai, Addison-Wesley
Modern Quantum Mechanics (1985)

[16] Robert Roth, TU Darmstadt
Skript zur Theoretischen Kernphysik

[17] D. Jaksch and P. Zoller
Annals of Physics **315**, *52-79 (2005)*

[18] Florian Gebhard
The Mott Metal-Insulator Transition
Springer Tracts in Modern Physics **137**

[19] Robert Roth and Keith Burnett
Phys. Rev. A **68**, *023604 (2003)*

[20] Robert Roth and Keith Burnett
Phys. Rev. A **67**, *031602 (2003)*

[21] Robert Roth and Keith Burnett
Phys. Rev. A **69**, *021601(R) (2004)*

[22] D. van Oosten, P. van der Straten and H.T.C. Stoof
Phys. Rev. Lett. A **63**, *053601 (2001)*

[23] Norio Kawakami and Sung-Kil Yang
Phys. Rev. B **44**, *7844 (1991)*

[24] O. Penrose and L. Onsager
Phys. Rev. **104**, *576 (1956)*

[25] C. N. Yang
Phys. Mod. Rev. **34**, *694 (1962)*

[26] M.P.A. Fisher, P.B. Weichmann, G. Grinstein and D.S. Fisher
Phys. Rev. B **40**, *546 (1989)*

[27] A. J. Legget
Phys. Mod. Rev. **71**, *S318 (1999)*

[28] G. G. Batrouni, V. Rousseau, R. T. Scalettar
Phys. Rev. B **46**, *9051 (1992)*

[29] J. K. Freericks and H. Monien
Phys. Rev. B **53**, *2691 (1996)*

[30] F. Gerbier, A. Widera, S. Fölling, O. Mandel, T. Gericke and I. Bloch
cond-mat/0503452

[31] Markus Hild
Dynamics of Atomic Gases in Modulated Optical Lattices,
Diploma Thesis, Technische Universität Darmstadt (2005)

[32] Karen Braun-Munzinger
Dynamics of Bose-Einstein Condensates in Optical Lattices,
PhD Thesis, University of Oxford (2005)

[33] Arpack Software
Source: http://www.caam.rice.edu/software/ARPACK/

Acknowledgements

First of all, I would like to thank Robert Roth for giving me the opportunity to become a member of his exciting TNP^{++} work group and for supervising the work on this diploma thesis. Without his endurance in answering my numerous questions this work would not have been possible.

I am much obliged to my colleagues: Markus Hild for his support in code writing and his help in understanding our field of work, Heiko Hergert for sharing his Mathematica and LaTeX skills and Dominik Nickel for many fruitful discussions. The rest of the TNP^{++} and NHQ members, as well as Genette Kluckner and David Ondreka provided an excellent and relaxing working environment.

Thanks to Hans Feldmeier for his advice that helped me to tackle many-particle quantum mechanics, and for his enriching lectures.

Special thanks go to my mother Monika for backing me all the way, at all times, to my brother Florian for encouraging me to make high demands on myself and of course to my girlfriend Alexandra Zill for undergoing my 'after-work-freak-outs' and simply for still loving me.

A lot of thanks is due to all my friends, in particular Stefan Friedrich and Jens Engemann for always reminding me of the life beyond physics.

Last but not least I want to thank the TUD Tae Kwon Do group for maintaining my mental and physical balance and my friends from T-Systems (BUDA) for providing the nice side job.